Stable isotope paleohydrology of pedogenic carbonates in the Wayan Formation (Albian) from the wedge-top depozone in the North American Cretaceous Western Interior Basin

By

Jeffrey Bryce Ross

Submitted to the graduate degree program in Geology and the Graduate Faculty of the University of Kansas in partial fulfillment of the requirements for the degree of Master of Science.

_____

Chairperson Gregory Ludvigson

_____

Andreas Möller

_____

Luis González

_____

J. Douglas Walker

Date Defended: August 23, 2016

The Thesis Committee for Jeffrey Ross

certifies that this is the approved version of the following thesis:

Stable isotope paleohydrology of pedogenic carbonates in the Wayan Formation (Albian) from the wedge-top depozone in the North American Cretaceous Western Interior Basin

Chairperson Gregory Ludvigson

Date approved: August 23, 2016

Abstract

Determining the presence and effects of orogenic rain shadows on paleoclimate is challenging, but critical to understanding overall moisture and heat transport. This thesis presents new data and interpretation for the climate system of the Cretaceous greenhouse world, which is a major keystone in Earth system science. Stable isotopic paleohydrologic data on mid-Cretaceous paleosols spanning from paleoequatorial sites in Colombia to paleoarctic latitudes in Alaska have been used to constrain the oxygen isotope mass balance of the Albian hydrologic cycle. At mid-latitudes (40-50°N paleolatitude), sideritic paleosols predominate, indicating paleoenvironments with positive precipitation – evaporation (P-E) balances, local exceptions with negative P-E balances occur on the immediate leeward side of the Sevier Orogen, where calcic paleosols in the wedge-top depozone record paleoenvironments with negative P-E balances in the orographic rain shadow. Stratigraphic sections in the Wayan Formation of Idaho (WF) were sampled from the wedge-top depozone. The units consist of stacked m-scale mudstone paleosols separated by m-scale sandstone-siltstone beds. Sections were sampled for organic carbon isotope profiles, and B-horizons from 6 well-developed paleosols were sampled for detrital zircons to determine maximum depositional ages. The first of these from the WF has produced a U-Pb concordia age of 101.0 ± 1.1 Ma, placing it in the uppermost Albian. This same WF section has produced a stratigraphic trend of upwardly decreasing $\delta^{13}C$ values ranging from -24 upwards to -27‰ VPDB, suggesting correlation to the late Albian C15 C-isotope segment. Pedogenic carbonates from the WF principally consist of micritic calcite, with carbon-oxygen isotope values that array along meteoric calcite lines (MCLs) with $\delta^{18}O$ values that range between -9.47 up to -8.39‰ VPDB. At approximately 42°N paleolatitude, these MCL values produce calculated paleoprecipitation values of -8.12 to -7.04‰ VSMOW, a range that is consistent with the estimates produced from other proxies at the same paleolatitudes across North America. These results indicate that despite the orographic rain shadow effect, the processes of meridional

atmospheric moisture transport in this locale were similar to those in more humid mid-latitude paleoenvironments elsewhere in the continent.

Acknowledgements

I would like to thank my field assistant, Stephan Oborny, for his help trenching and collecting samples, Luke Miller for his assistance processing samples. I would also like to thank Ted Dyman for walking me through a section of the Blackleaf Formation, and L. J. Krumenaker and Dave Varricchio of Montana State University for assistance in locating suitable Wayan Formation outcrops. And thanks to: Adrienne Duarte, Tony Layzell, Josh Feldman, Ty Tenpenny, and Maggie Graham for the training they provided to help me process samples. I would like to personally thank my advisor, Greg Ludvigson for the support he provided when work was not proceeding as planned. Many thanks to my committee members, Dr. González, Dr. Möller, and Dr. Walker for the help they provided in data interpretations. And I would like to say thank you to the entire Geology Department at The University of Kansas and the Alumni who offer grants and scholarships to help graduate students fund their research, specifically: Joseph M. Patterson Scholarship, Encana Energy Scholarship, Devon Energy Scholarship, Roy and Freda Lehman Scholarship, Gerhard Student Prize for Field Research in Geology, and AWG Osage Chapter for their generous donations.

Table of Contents

Chapter 1: Preface

Original Scope of Project and Condensed Thesis

The original thesis project was planned as an investigation of $\delta^{13}C$ and $\delta^{18}O$ of pedogenic carbonates and $\delta^{13}C_{org}$ of 50 meters of measured section of the Blackleaf Formation in the Lima Peaks region of Beaverhead County of southwestern Montana and the Wayan Formation in the Caribou Basin of Bonneville County of eastern Idaho. Detrital zircon sampling was also planned to aid in obtaining maximum depositional ages (MDA) of paleosol horizons, which contained pedogenic carbonate nodules. A total of 38 meters was trenched and sampled from 4 locations in the Blackleaf Formation and a total of 50 meters was trenched and sampled from 3 transects of the Wayan Formation. Research from a continuous 27 meter measured section of the Wayan Formation was presented at the International Geoscience Programme (IGCP) 609 at Nanjing University, China in September, 2015. After presenting, I was asked to contribute a manuscript to an IGCP609 special issue to be published in *Science China Earth Sciences* (Springer). After discussion with my advisor, it was decided to condense the scope of my thesis based on my submitted manuscript for publication. Within the manuscript submitted, the 27 meter section of the Wayan Formation presented 57 sampled calcite components from 3 of 7 total pedogenic carbonate nodules, $\delta^{13}C_{org}$ covering the 27 meters of measured section from 41 of 55 sampled horizons (not all samples yielded reliable data), and 283 analyses of detrital zircons from one sample horizon of the Wayan Formation. The submitted manuscript was co-authored with Drs. Greg Ludvigson (thesis committee chair who suggested and guided the project), Luis Gonzalez (thesis committee member and Director of the University of Kansas Keck Paleoenvironmental and Environmental Stable Isotope Laboratory who guided quantitative treatment of stable isotopic data), Doug Walker (thesis committee member and Director of the University of Kansas Isotope Geochemistry Laboratory and co-author for the Cretaceous time scale used in the manuscript), and Andreas Möller (thesis committee member and

supervisor of the University of Kansas laser-ablation ICP-MS laboratory who guided the collection, analysis, and presentation of the zircon U-Pb data).

Chapter 2: Submitted Manuscript for Publication

Introduction

Stable isotope investigations of the Cretaceous hydrologic cycle are yielding new insights into the role of atmospheric moisture and latent heat transport in regulating earth surface temperatures in an ancient greenhouse world (Ufnar et al., 2002, 2004; Suarez et al., 2009, 2011; Ludvigson et al., 2013). These include stable isotope data produced from pedogenic carbonates and phosphate substrates from vertebrate fossils. Much of the published mid-latitude data comes from pedogenic siderites that formed in paleo-environments with positive precipitation - evaporation (P-E) balances (Ufnar et al., 2002, Ufnar et al., 2004; Suarez et al., 2011). Within the Ferrel Cell, a zonal humid belt of the mid-latitudes, are local paleoenvironments related to orographic rain shadow effects on the leeward side of the Cretaceous Sevier Orogen (Fig. 1). The Wayan Formation of eastern Idaho is a continental deposit that accumulated in this local setting.

The Wayan Formation (WF) of the Caribou Basin in Idaho, U.S.A. (Fig. 2) has been described as a sequence of interbedded conglomerates, sandstones, siltstones, mudstones, and limestones that were deposited on an alluvial plain (Schmitt & Moran, 1982). Strata of the WF outcrop as sub-vertically dipping beds due to faulting and folding associated with accumulation on the wedge-top depozone, where deformation occurred near the depositional surface and not in a more deep burial setting (DeCelles & Giles, 1996). This alluvial plain in which the WF was deposited falls on the immediate leeward side of the Sevier Orogen. Atmospheric moisture transport by paleowesterlies would have been deflected by the Sevier Orogen and adiabatic warming of air masses descending on the leeward side of the orogen produced an orographic rain shadow as described by Elliott et al. (2007). Paleoclimate proxies at or near the same paleo-latitude as the WF indicate a warm temperate climate with the development of coals and kaolinites (Boucot et al., 2013), however, within the mid-latitude orographic rain shadow, a north-south trending fairway of calcrete deposits capture a record

of a semiarid paleoenvironment (Fig. 1). This project is based on ongoing research on the paleoenvironment and paleoclimate of the North American Cretaceous western interior basin (WIB), following from earlier studies that deciphered the paleoenvironments, paleoecology, and paleoclimate of the Cretaceous WIB utilizing isotopic compositions of fossilized vertebrate faunas (Suarez et al., 2012, 2014), siderites (Ufnar et al., 2002), and soil formed carbonate nodules (Ludvigson, et al., 2010). The aforementioned examples have helped further our knowledge about the paleoclimatology of the Cretaceous WIB. However, within the zonal humid belt in mid-latitude North America, there are localized semi-arid environments in the rain shadow of the Sevier Orogen. These locales need further study to clarify mechanisms of atmospheric vapor transport to understand why they are different.. Pedogenic carbonate nodules that *formed in situ* within paleosols of the WF can provide isotopic data from a semiarid paleoenvironment within the rain shadow of the Sevier Orogen to contrast with previously published data from the Cretaceous WIB.

Global chemostratigraphic profiles of marine carbonates ($\delta^{13}C_{carb}$) and organic carbon ($\delta^{13}C_{org}$) have been correlated through the Aptian-Cenomanian, identifying carbon isotope excursions (CIEs) associated with oceanic anoxic events (OAEs; Scholle and Arthur, 1983; Leckie et al., 2002). A carbon isotope chemostratigraphic profile of from the WF has been produced to compare with published profiles to expand on developing knowledge of organic carbon chemostratigraphy within the terrestrial realm. Correlating global CIEs with those identified in the chemostratigraphic profile of the WF requires integration with radiometric U-Pb dates.

Previously-published stratigraphic studies of the WF have used biostratigraphic correlations to place the WF within the Albian and Cenomanian (Krumenacker et al., 2016). Geochronological data integrated with carbon isotope chemostratigraphy of paleosols is a developing approach that can be used to constrain time in the terrestrial realm. Previous work with volcanogenic zircons has dated the Wayan Formation to between 95.5 and 101.8 Ma (Krumenacker, 2010). An important aspect of

this project is therefore U-Pb dating of zircon from paleosol horizons within a measured section to provide maximum depositional ages (MDA) of the sampled horizons.

Methods

Wayan Formation Outcrop

Sampling of the WF took place in the Caribou Basin of Bonneville County in eastern Idaho (Fig. 2B). A 27 meter composite measured section was trenched perpendicular to strike which ranged from N10°W to N15°W (dip angles from 80 to 90° east) through this section along McCoy Creek Road at 43.1478° N, 111.2479° W. Trenches along the outcrop were dug to approximately 0.5 meters depth below surface to collect samples that have not been exposed to surficial weathering processes.

Pedogenic Carbonate Nodules

Pedogenic carbonate nodules were collected from 7 well developed paleosol B-horizons of the WF. Matching micropolished thin and thick sections were cut from epoxy resin-impregnated billets for petrographic analysis. Cathodoluminescence (CL) imaging was used to identify variably luminescent and non-luminescent calcite components on thick sections. Photomicrographs were produced in CL and mapped onto reflected light (RL) images to guide microsampling of various calcite components for $\delta^{13}C$ and $\delta^{18}O$ analyses (Figure 3 A-C).

Cathodoluminescence imaging was carried out at the Kansas Geological Survey Digital Cathodoluminescence Imaging Laboratory using a Reliotron III cold cathode chamber mounted on a Relion Industries table top stand. Macroimages were captured with a Canon EOS Xti 10.1 Mpx DSLR using a Canon EFS 60mm f/2.8 macro USM lens mounted on a boom stand suspended over the CL chamber. CL images were captured in operating conditions that consisted of an electron beam voltage of 10 kV, a beam current of 0.5 mA, and in a chamber with rarified Helium atmosphere at 50 milliTorr.

Pedogenic carbonate components were micro-sampled at The University of Kansas Keck-NSF Paleoenvironmental and Environmental Laboratory. Each carbonate component identified was sampled from 2 to 5 separate locations on each nodule. A minimum of 100 µg of sample was collected from each sample location (Fig. 3) and was shipped to the University of Michigan Stable Isotope Laboratory for analyses on a Finnigan MAT 251 coupled to a Finnigan Kiel automated preparation device (Appendix C). Cross-plots of $\delta^{13}C$ and $\delta^{18}O$ values were made and used to interpret diagenetic history for sampled nodules (Fig. 4). The MCL values obtained from carbonate nodules of the WF will be used calculate paleoprecipitation $\delta^{18}O$ values for comparison with other published paleoprecipitation $\delta^{18}O$ values (Suarez et al., 2009; Fig. 5). This comparison will determine whether or not paleogroundwater and paleoprecipitation $\delta^{18}O$ values from the WF are comparable to those determined from pedogenic siderites at the same paleolatitudes (42-43° north) elsewhere in North America. This will be the first study to determine if isotopic data from the orographic rain shadow of the Sevier orogen produces proxy data that are comparable to paleohydrologic and paleoclimatic data from more humid paleoenvironments in the Cretaceous North American mid latitudes presented by Suarez et al., (2009).

Organic Carbon Isotopes

A 27 meter section of the Wayan Formation was sampled at 0.5 meter intervals for organic carbon isotope analyses. Samples were ground in a ceramic mortar and pestle and dried over a 24 hour period before being placed into centrifuge tubes. Tubes were weighed before and after adding samples to allow for a total organic carbon (TOC) percent to be calculated after analyses. Samples were then acidified with 0.5N HCl to remove carbonate and leached to a neutral pH. Acidified samples were combusted in Costech Elemental Analyzer coupled to continuous-flow ThermoFinnigan MAT 253 stable isotope ratio mass spectrometer at the Keck Paleoenvironmental & Environmental Stable Isotope Laboratory at The University of Kansas to produce organic $\delta^{13}C$ analyses (Appendix B). Standards used to calibrate the $\delta^{13}C$ the analyses were USGS-24 (graphite),

DORM (dogfish muscle), IAEA-600 (caffeine), ANU (sucrose), MT soil, and Peach Leaf. The organic carbon $\delta^{13}C$ values are plotted with stratigraphic profiles to assess the chemostratigraphic structure of studied units (Fig.5).

U-Pb geochronology of zircon

Bulk paleosol samples of 2-3 kg were collected from sample horizons in the WF that contained carbonate nodules. Samples were split to reduce bulk size to 1 kg. Due to high concentrations of calcite cement the samples were initially acidified with 1.5N HCl to aid the disaggregation process. After decarbonation, the samples were crushed and a GEMENI mineral concentration table was used to separate the majority of light minerals from the higher density minerals, including zircon. An iodine bath was used to remove remaining clays from mineral grain surfaces. Zircon was concentrated with methylene iodide heavy liquid and a Frantz isodynamic magnetic separator. A total of 310 zircon grains were hand-picked under a binocular microscope, mounted in an epoxy resin disc, and micropolished to expose grain surfaces in order to ensure analysis of the youngest stage(s) of zircon crystal growth. Some zircon grains were not analyzed due to little to no surface exposure in the epoxy resin disc. A total of 283 zircon grains were analyzed with a Thermo Scientific Element2 ICP-MS, attached to a Photon Machines Analyte.G2 193 nm ArF excimer laser ablation system. 20 µm circular spots were ablated with 2.0 J cm^{-2} fluency and a 10 Hz repetition rate, which produced ablation pits of ca. 10 µm depth. The ablated material was carried to the ICP in He gas with a 1.1 l min^{-1} flow rate, tied into a ca. 1.1 l Ar flow just before entry into the plasma torch. Elemental fractionation, downhole fractionation and calibration drift were corrected by bracketing measurements of unknowns with GJ1 zircon reference material (Jackson et al., 2004). Data reduction was carried out with the IOLITE software package (Paton et al., 2010; 2011) using the VizualAge data reduction scheme (Petrus and Kamber, 2012). The reproducibility of the GJ1 reference material used for calibration (Jackson et al., 2004) during the analytical session was better than 0.2 % on the $^{206}Pb/^{238}U$ age (weighted average 600.4 ± 1.2 Ma, MSWD = 0.33, n = 58), which

was propagated into the uncertainty of the unknowns. Plesovice zircon (Slama et al. 2008) was used as a secondary reference material to assess age accuracy and 26 concordant analyses yielded a concordia age of 340.7 ± 1.0 Ma, with an MSWD of 0.79. This is within 1% of the thermal ionization mass spectrometry results of Slama et al. (2008) and within error identical to the $^{206}Pb/^{238}U$ age of 340.94 ± 0.53 Ma determined by six other LA-ICP-MS and SIMS laboratories that yielded reliable results for a variety of reference materials in the study of Kosler et al. (2013). All data obtained on 283 zircon grains are shown in Appendix A, but only concordant or near-concordant analyses were used for plots and calculations. The filtering for discordant analyses was done by two different calculations. For grains with $^{206}Pb/^{238}U$ dates below 900 Ma, results were excluded that had values above 1.2 for: ($^{207}Pb/^{235}U$ date - $^{206}Pb/^{238}U$ date) / $^{207}Pb/^{235}U$ 2SE. This takes into account that in LA-ICP-MS U-Pb analysis of young zircon, the $^{207}Pb/^{235}U$ date has a high uncertainty due to the low abundance of ^{207}Pb. For grains with $^{206}Pb/^{238}U$ dates above 900 Ma discordance % was calculated as: (1 - ($^{207}Pb/^{206}Pb$ date / $^{206}Pb/^{238}U$ date)) x 100, and data more than 5% discordant were excluded from plots and further discussion. Of the 283 results 209 analyses passed these two discordance filters.

Results

Petrography and Stable Isotope Data for Pedogenic Carbonates

Pedogenic carbonates from sample WN1.2 consist of nodule matrix components that are characterized by radial fibrous microspar with micron-scale speckled cathodoluminescence (CL) luminescence, and with long crystal dimensions from 100 to 800 µm (Fig. 3A). Septarian veins contained within nodules from WN1.2 are filled by zoned calcite spars with distinctive CL characteristics. The first of these, Zone 1, consists of non-luminescent septarian vein calcites with equant crystal dimensions of about 100-200 µm that are present on the edges of septarian veins and matrix components, and completely fill smaller septarian veins (Fig. 3A). The following Zone 2 consists of dully luminescent equant calcite crystals with dimensions ranging between 100 to 500 µm

that are present in larger septarian veins between zone 1 and zone 3 septarian veins (Fig. 3A). The later Zone 3 consists of brightly luminescent equant calcite crystals with crystal dimensions ranging between 500 to 2000 µm and occurs as the final phase of septarian vein calcite crystal growth (Fig. 3A).

Pedogenic carbonate nodules from sample WN1.3 consist of smaller nodules with a non-luminescent micritic matrix calcite, with crystal dimensions of less than 10 µm; these smaller nodules are encompassed within larger nodules with dully-luminescent micritic matrix, with crystal dimensions less than 20 µm (Fig. 3B). Nodules from WN1.3 also contain zoned septarian veins that are filled by successive zones of calcite spars with distinctive CL characteristics. The earliest Zone 1 consists of dully luminescent equant calcite with crystal dimensions ranging between 50 to 250 µm – these occur within the septarian veins of smaller micritic nodules contained within the larger nodules, and also within septarian veins of the encompassing larger nodules (Fig. 3B). The later Zone 2 consists of brightly-luminescent equant crystals with dimensions ranging from 100 and 800 µm that occur in the largest septarian veins within the larger micritic nodules (Fig. 3B).

Pedogenic carbonates from sample WN1.5 consists of nodule matrix components that display a radial fibrous microspar characterized by a micron-scale speckled luminescence, with long crystal dimensions from 100 to 800 µm (Fig. 3C). Septarian veins contained within nodules from WN1.5 are filled by zoned calcite spars with distinctive CL characteristics. The earliest Zone 1 consists of non-luminescent septarian vein calcites with equant crystal dimensions of about 100-200 µm, and are present along the edges of matrix components along vein walls (Fig. 3C). The later Zone 2 consists of luminescent equant calcite crystals with dimensions ranging between 100 to 500 µm that are present in larger septarian veins between zones 1 and 3 (Fig. 3C). Zone 3 consists of brightly luminescent equant calcite crystals with dimensions ranging between 500 to 2000 µm and occur in the centers of larger septarian veins as the final phase of calcite crystal growth (Fig. 3C).

The paragenetic sequence of carbonate diagenesis in the nodules was initiated by precipitation of carbonate matrix components. Early non-luminescent septarian vein calcites precipitated within a shallow phreatic groundwater system on the basis of equant crystal morphologies; later brightly luminescent septarian vein calcites precipitated in deeper phreatic groundwater setting where higher concentrations of Mn^{2+} in anoxic pore fluids were incorporated within septarian vein calcites.

Carbonate nodules from the Wayan Formation contain matrix calcite components that produce relatively invariant oxygen isotope values. They are arrayed along MCL trends (*sensu* Lohmann, 1988), a pattern that can develop in pedogenic calcites in modern surface soils (Mintz et al., 2011). The MCL trends of the Wayan Formation have $\delta^{18}O$ values that range from -9.47 ± 0.64‰ up to -8.39 ± 0.21‰ VPDB, with three examples of carbon-oxygen isotope plots shown in Figure 4. Later-stage brightly-luminescent septarian vein calcites (Zone 3) have notably lower $\delta^{18}O$ values ranging from -16.56 to -10.93‰ VPDB, while the $\delta^{13}C$ values of Zone 3 calcites are similar to those of the enclosing finer-grained matrix calcites (Fig. 4A-4C).

Organic Carbon Isotope Chemostratigraphy

A $\delta^{13}C_{org}$ chemostratigraphic profile of the WF (Fig. 5) displays a stratigraphic upward trend from higher values at the base (about -23‰ VPDB) to lower values at the top of the section (about -27‰ VPDB). Several minor carbon isotope fluctuations can be seen within three point moving average of the $\delta^{13}C_{org}$ profile (Fig. 5), specifically at the 9 meter interval where there is an early negative shift to -26.49‰ followed by a maximum positive shift at the 15.5 meter interval to -22.0‰ before returning to a negative trend to the end of the profile. However, the chronostratigraphic significance of these features is uncertain without additional geochronologic data from other parts of the sampled section.

U-Pb geochronology of zircon from sample WN1.5

Two hundred eighty three U-Pb analyses were performed by LA-ICP-MS on detrital zircon from the WF obtained from sample location WN1.5 at 11.6 meters above the base of the section (Fig. 5). A total of 209 of the analyzed grains passed the concordance criteria outlined in the methods chapter above, and 58 of these are younger than 200 Ma (Fig. 6A). Fifty-five of these fall in a narrow range of latest Early Cretaceous (Albian) age with $^{206}Pb/^{238}U$ dates from 99.7 to 113.2 Ma (Fig. 6A), whereas only one Aptian, one Late Jurassic and one Early Jurassic grain were found. A U-Pb Concordia age of 101.0 ± 1.1 Ma was calculated from the youngest 3 concordant zircon analyses overlapping within error (Fig. 6B), which is interpreted as the best estimate for the maximum depositional age (MDA) of the sampled stratum (after the strategy proposed by Dickinson & Gehrels, 2009). The distribution of results within the Early Cretaceous population is shown in a kernel density plot (kdp) produced with the DensityPlotter software (Vermeesch, 2012), which shows a major age distribution maximum at ca. 105 Ma, with a slightly skewed distribution and a local maximum of results at ca. 110 Ma (Fig. 6C).

Among the pre-Cretaceous zircon grains, only one late Triassic (Rhaetian) zircon, and no concordant zircons with ages between 205 and 300 Ma were found. The full distribution of concordant detrital zircons with ages between 130 Ma and 3.0 Ga is shown in a kdp in Fig. 6D. The oldest concordant analyses (3671 ± 87 Ma) is not shown in Fig. 6D to conserve space in the figure. Notable maxima in the age distribution are found in the Late Devonian at ca. 380 Ma, early Silurian at ca. 440 Ma, and early Ediacaran at 600 to 650 Ma. Lower abundances of grains were found to have a broad distribution of ages between ca. 800 Ma and 2000 Ma. The most prominent of these small maxima is at ca. 1.6-1.7 Ga. Isolated single zircons with ages at 2.2, 2.6, and 2.7 Ga, and 2 analyses at 2.8 Ga were obtained.

Discussion

Primary calcite components from pedogenic nodules in the Wayan Formation that capture early diagenetic paleohydrologic information are the non-luminescent to dully luminescent micritic matrix, and radial fibrous microspars with speckled luminescence (Fig. 3A-3C). These components yield carbon and oxygen isotope values that array along MCL trends, and are interpreted to be precipitated from shallow groundwaters sourced from infiltrating paleoprecipitation in the ancient vadose zones of mid-Cretaceous paleosols. Zone 1 cathodoluminescence (CL) non-luminescent spars filling septarian veins have carbon and oxygen isotope values that are closely-similar to matrix carbonates. Post-burial diagenetic components are represented by septarian vein calcites, Zone 2 luminescent and Zone 3 brightly luminescent spars (Fig. 3A-3C). These later diagenetic components formed in anoxic groundwaters that incorporated reduced manganese into the calcite crystal lattice. Paleohydrologic interpretations for individual stratigraphic horizons are developed through the analysis of specific diagenetic trends identified in $\delta^{13}C$ and $\delta^{18}O$ cross plots, and are unique to each studied rock sample (Fig. 4A-4C)). Diagenetic trends include meteoric calcite lines (MCLs) that preserve records of the $\delta^{18}O$ compositions of infiltrating paleoprecipitation (Lohmann, 1988; Ludvigson et al., 2010). Later diagenetic trends include the records of burial diagenesis captured by Zone 3 brightly luminescent septarian vein calcite spars, showing a trend toward lower $\delta^{18}O$ values. Zone 3 calcite spars have similar $\delta^{13}C$ values as the matrix calcites, suggesting formation in a rock-dominated diagenetic system (Lohmann, 1988; Fig. 4A-4C). This O-isotopic value could be indicative of infiltration of groundwaters sourced by alpine snowmelt, or alternatively, could be indicative of precipitation at higher burial temperatures, as posited by Ludvigson et al. (2010; 2015) and Suarez et al. (2014).

The paleolatitude of 42° N for the Wayan Formation was estimated based on paleogeographic reconstructions of Aptian-Albian North America by Ufnar et al. (2004).

The local mean annual paleotemperature (MAPT) was calculated from the second-order polynomial regression generated by Ufnar et al. (2002) based on a Cretaceous latitudinal temperature gradient reported by Spicer and Corfield (1992) and fossil leaf physiognomy data of Wolfe and Upchurch (1987). This same approach was used by Suarez et al. (2009):

$$t = 30.25 - 0.2025l - 0.0006l^2,$$

where t is temperature in degrees Celsius, and l is latitude, produced a MAPT of 21.74° C. Using this paleotemperature, the $\delta^{18}O$ VPDB MCL values from the WF can be used to calculate $\delta^{18}O$ VSMOW values of infiltrating paleoprecipitation. MCL values from carbonate matrix components from nodules of the WF yield estimated meteoric water values that range from -8.12 to -7.04‰ VSMOW (Fig 4D). These estimated groundwater $\delta^{18}O$ values are consistent with those estimated from pedogenic siderites (Ufnar et al., 2002), from pedogenic calcites (Ludvigson et al. 2004), and $\delta^{18}O$ isotopic data from vertebrate fossil phosphate substrates (Suarez et al. 2012, 2014).

With the maximum depositional age (MDA) determined at 101.0 ± 1.1 Ma at the end of the Albian Stage, it is possible to accurately correlate CIEs of the WF with established global Aptian-Albian chemostratigraphic profiles (Fig. 7). The base of the WF $\delta^{13}C$ chemostratigraphic profile, beginning at the zero meter line, shows a general decreasing isotope trend from -23.32 to -26.49‰ VPDB over a 9 meter interval (Fig. 7). Above this trend of decreasing values, a positive isotope trend occurs up to the 14.5 meter interval with an abrupt increase over the next two sample positions to the 15.5 meter sample interval, where the most positive $\delta^{13}C$ occurs at -22‰ (Fig. 7). Following this high value, there is an upward trend of decreasing $\delta^{13}C$ values through the remainder of the section to ending values of about -27‰ VPDB (Fig. 7). The MDA of 101.0 ± 1.1 Ma established from detrital zircons obtained from the 11.6 m interval of the $\delta^{13}C$ profile of the WF permits correlation with global Aptian-Albian $\delta^{13}C$ profiles of Leckie et al. (2002) in the late Albian, and

intersect with the $\delta^{13}C_{org}$ C15 C-isotope segment originally identified by Bralower et al. (1999). The C15 C-isotope segment of Bralower et al. (1999) has two minor negative C isotope shifts occurring within an overall positive C isotope trend (Fig. 7). The MDA obtained from the detrital zircon U-Pb age of 101.0 Ma places the WF $\delta^{13}C$ profile between the two minor negative shifts of the Bralower et al. (1999) C15 C-isotope segment (Fig. 7).

The $\delta^{13}C$ decrease in the WF C-isotope profile occurring up to the 9 meter interval might be correlated with the first C15 negative shift, with the most positive C-isotope value recorded at the 15.5 meter interval of the WF correlating with the following positive shift from Bralower et al. (1999). The upper 11.5 meters of the WF $\delta^{13}C$ profile shows an overall declining $\delta^{13}C$ trend, and may correlate with the second minor negative shift within the C15 isotope segment of Bralower et al. (1999). With 5 other zircon samples currently being processed, the full $\delta^{13}C$ profile of the WF can be more confidently correlated with global Aptian-Albian $\delta^{13}C$ chemostratigraphic profiles to further constrain time in the WF.

The abundant Albian zircon population (26% of all concordant analyses) is interpreted to reflect the highly active magmatic arc in very proximal westerly distance from the sample location (e.g. Fig. 2A). The paucity of earlier Mesozoic and Permian zircons may reflect the general east- and northward transport direction at the sample location that prevented capture of any zircons from a source east of the North American Cretaceous Western Interior Seaway during this time period. Carboniferous and older zircons could have been transported far west from the East during earlier times when different transport directions dominated, and then redistributed later, as proposed e.g. by Blum & Pecha (2014) for the presence of Appalachian-age zircon throughout the Midwestern US and Central Canada. The pattern of Proterozoic zircon in the WN1.5 sample from Idaho generally matches very well with detrital zircon data from Albian strata from the Western Canada Sedimentary Basin in Northern Alberta (Blum & Pecha, 2014), with moderate amounts of Grenvillean, Mid-Continent and Yavapai-Mazatzal input. The Early Proterozoic to Eoarchean oldest obtained ages

may be derived from relatively proximal underlying basement sources, the Wyoming province in the southeast or the Medicine Hat Block directly to the west and their adjacent Early Proterozoic orogenic belt neighbors (see Whitmeyer & Karlstrom 2007), although Eoarchean material is generally extremely rare.

Conclusions

- Pedogenic carbonate nodules of the Wayan Formation produce carbon and oxygen isotope data that array along meteoric calcite lines (MCLs), with $\delta^{18}O$ values ranging from -9.47 ± 0.35‰ to -8.39 ± 0.58‰ VPDB. These MCL values produce calculated meteoric water values ranging from -8.12 to -7.04‰ VSMOW. Estimated paleoprecipitation/paleogroundwater $\delta^{18}O$ values from the Wayan Formation are similar to those estimated from other published Albian paleoprecipitation proxies at about 42° N paleolatitude. These results suggest that meridional atmospheric moisture transport in the rain shadow on the leeward side of the Cretaceous Sevier Mountain was similar to that elsewhere in the North American Western Interior Basin.
- Mudstone paleosols of the Wayan Formation produce an organic carbon isotope chemostratigraphic profile that exhibits an overall decreasing trend from bottom to top.
- A U-Pb concordia age of 101.0 ± 1.1 Ma was calculated from a bulk paleosol sample at the 11.6 meter horizon from the Wayan Formation. The 101.0 ± 1.1 Ma age was produced from the youngest 3 concordant detrital zircons overlapping within 2σ. Following the logic of Dickinson and Gehrels (2009), 101.0 ± 1.1 Ma is proposed as the maximum depositional age for this sample horizon and facilitates correlation of the $\delta^{13}C$ profile from the Wayan Formation to the global Cretaceous C-isotope stratigraphy.
- Applying the MDA of 101.0 ± 1.1 Ma to the $\delta^{13}C$ profile of the Wayan Formation (WF), comparison to the global Cretaceous (Aptian-Albian) C-isotope stratigraphy indicates that the WF $\delta^{13}C$ profile correlates to the C15 C-isotope segment identified by Bralower et al. (1999).

Within the $\delta^{13}C$ profile of the WF there are more short-term trends of decreasing and increasing $\delta^{13}C$ values that might correlate to minor C-isotope shifts within the C15 C-isotope segment of Bralower et al. (1999). More geochronologic data are needed to further constrain the chronostratigraphy of these C-isotope trends.

Chapter 3: Future Work

Continuation of Thesis Research

Wayan Formation

This initial measured section from the Wayan Formation (WN site 1) has 5 more bulk paleosol samples, which are being processed for detrital zircon analyses, and has 4 more pedogenic carbonate nodules consisting of 75 additional $\delta^{13}C$ and $\delta^{18}O$ carbonate mineral analyses that were not included in this submitted manuscript, but will be included in future publications when zircon analyses are completed.

Wayan Formation site 2 (WN-2) is a 13 meter measured section consisting of 27 $\delta^{13}C_{org}$ analyses that have been completed and paired with a stratigraphic profile. The WN-2 measured transect also contains one pedogenic carbonate nodule horizon for which 26 $\delta^{13}C$ and $\delta^{18}O$ carbonate mineral analyses have been completed. A bulk paleosol sample from WN-2 collected at the carbonate nodule horizon is being processed for detrital zircon analyses.

Wayan Formation site 3 (WN-3) is a 10 meter measured section with 21 $\delta^{13}C_{org}$ analyses which have been completed and paired with a stratigraphic profile. The WN-3 measured transect also contains one pedogenic carbonate nodule horizon for which 18 $\delta^{13}C$ and $\delta^{18}O$ carbonate mineral analyses have been completed. A bulk paleosol sample from WN-3 collected at the carbonate nodule horizon is being processed for detrital zircon analyses.

Blackleaf Formation

Sampling of the Blackleaf Formation was completed with initial field work in 2013. Four measured sections totaling 38 meters include 80 $\delta^{13}C_{org}$. Three of the four measured sections contained pedogenic carbonate nodule horizons for which 76 $\delta^{13}C$ and $\delta^{18}O$ carbonate mineral analyses have been completed. All 4 measured sections also include one bulk paleosol horizon from each section that are currently being processed for detrital zircon analyses.

Future Plans for Publication

Following the completion of detrital zircon U-Pb analyses, unpublished data from measured sections of the Wayan Formation and the Blackleaf Formation will be reported on in relevant peer reviewed journals as part of continuing research into paleoclimatology during my PhD tenure at The University of Kansas.

References

Blakey R. 2014. Library of Paleogeography. Retrieved April 4, 2016, from Colorado Plateau Geosystems, Inc.:http://cpgeosystems.com/images/WNA_100_KAlb-sm.jpg

Blum M, Pecha M. 2014. Mid-Cretaceous to Paleocene North American drainage reorganization from detrital zircons. Geology, 42(7): 607-610. doi:10.1130/G35513.1

Boucot A J, Xu C, Scotese C R. 2013. Phanerozoic paleoclimate: an atlas of lithologic indicators of climate. Concepts in Sedimentology and Paleontology 11: SEPM (Society for Sedimentary Geology): 216-217. Tulsa, OK, U.S.A.

Bralower T, CoBabe E, Clement B, et al. 1999. The record of global change in mid-Cretaceous (Barremian-Albian) sections from the Sierra Madre, northeastern Mexico. Journal of Foraminiferal Research, 29(4): 418-437.

DeCelles P G, Giles K A. 1996. Foreland basin systems. Basin Research, 8(2): 105-123.

Dickinson W R, Gehrels G E. 2009. Use of U-Pb ages of detrital zircons to infer maximum depositional ages of strata: a test against a Colorado Plateau Mesozoic database. Earth and Planetary Science Letters, 288(1-2): 115-125. doi:10.1016/j.epsl.2009.09.013

Elliot W S, Suttner L J, Pratt L M. 2007. Tectonically induced climate and its control on the distribution of depositional systems in a continental foreland basin, Cloverly and Lakota Formations (Lower Cretaceous) of Wyoming, U.S.A. Sedimentary Geology, 202: 730-753. doi:10.1016/j.sedgeo.2007.09.001

Erbacher J, Thurow J, Littke R. 1996. Evolution patterns of radiolaria and organic matter variations: a new approach to identify sea-level changes in mid-Cretaceous pelagic environments. Geology, 24(6): 499-502. doi:10.1130/0091-7613(1996)024<0499:EPORAO>2.3.CO;2

Jackson S E, Pearson N J, Griffin W L, et al. 2004. The application of laser ablation-inductively coupled plasma-mass spectrometry to in situ U-Pb zircon geochronology. Chemical Geology, 211(1-2): 47-69. doi:10.1016/j.chemgeo.2004.06.017

Košler J, Sláma J, Belousova E, et al. 2013. U-Pb detrital zircon analysis - results of an inter-laboratory comparison. Geostandards and Geoanalytical Research, 37(3): 243-259. doi:10.1111/j.1751-908X.2013.0245.x

Krumenacker L J. 2010. Chronostratigraphy and paleontology of the mid-Cretaceous Wayan Formation of eastern Idaho, with a description of the first oryctodromeus specimens from Idaho. Thesis for Master's Degree. Retrieved January 29, 2013, from Electronic Theses & Dissertations: http://contentdm.lib.byu.edu/cdm/ref/collection/ETD/id/2317

Krumenacker L J, Simon D J, Scofield G, et al. 2016. Theropod dinosaurs from the Albian-Cenomanian Wayan Formation of eastern Idaho. Historical Biology: 1-17. doi:10.1080/08912963.
2015.1137913

Leckie M, Bralower T, Cashman R. 2002. Oceanic anoxic events and plankton evolution: biotic response to tectonic forcing during the mid-Cretaceous. Paleoceanography, 17(3). doi:10.1029/2001PA000623

Lohmann K C. 1988. Geochemical patterns of meteoric diagenetic systems and their application to studies of paleokarst. Paleokarst: 58-80.

Ludvigson G A, González L A, Fowle D A, et al. 2013. Paleoclimatic applications and modern process studies of pedogenic siderite. New Frontiers in Paleopedology and Terrestrial Paleoclimatology. SEPM Special Publication, 104: 79-87.

Ludvigson G A, González L A, Kirkland J I, et al. 2003. A mid-Cretaceous record of carbon isotope excursions in palustrine carbonates of the Cedar Mountain Formation of Utah: marine-terrestrial

correlations of Aptian-Albian oceanic anoxic events 1a, 1b, and 1d. The 3rd International Limnology Congress, Abstract Volume, 169.

Ludvigson G A, Joeckel R M, Murphy L R, et al. 2015. The emerging terrestrial record of Aptian-Albian global change. Cretaceous Research, 56: 1-24. doi: 10.1016/j.cretres.2014.11.008

Ludvigson G A, Joeckel R M, González L A, et al. 2010. Correlation of Aptian-Albian carbon isotope excursions in continental strata of the Cretaceous foreland basin, eastern Utah, U.S.A. Journal of Sedimentary Research, 80: 955-974. doi:10.2110/jsr.2010.086

Ludvigson G A, Ufnar D F, González L A, et al. 2004. Terrestrial paleoclimatology of the mid-Cretaceous greenhouse I: cross-calibration of pedogenic siderite & calcite $\delta^{18}O$ proxies at the Hadley cell boundary. Geological Society of America Abstracts with Programs, 36(5): 305.

Mintz J S, Driese S G, Breeker D O, et al. 2011. Influence of changing hydrology on pedogenic calcite precipitation in vertisols, Dance Bayou, Brazoria County, Texas, U.S.A.: implications for estimating paleoatmospheric pCO_2. Journal of Sedimentary Research, 81: 394-400. doi:10.2110/jsr.2011.36

Paton C, Hellstrom J, Paul B, et al. 2011. Iolite: Freeware for the visualization and processing of mass spectrometric data. Journal of Analytical Atomic Spectrometry, 26(12): 2508-2518. doi:10.1039/
C1JA10172B

Paton C, Woodhead J D, Hellstrom J C, et al. 2010. Improved laser ablation U-Pb zircon geochronology through robust downhole fractionation correction. Geochemistry, Geophysics, Geosystems, 11(3). doi:10.1029/2009GC002618

Petrus J A, Kamber B S 2012. VizualAge: A novel approach to laser ablation ICP-MS U-/Pb geochronology data reduction. Geostandards and Geoanalytical Research, 36(3): 247-270. doi:10.1111/j.1751-908X.2012.00158.x

Schmitt J, Moran M. 1982. Stratigraphy of the Cretaceous Wayan Formation, Caribou Mountains, southeastern Idaho thrust belt. Rocky Mountain Geology, 21(1): 55-71.

Scholle P A, Arthur M A, Ekdale A A. 1983. Pelagic environment. American Association of Petroleum Geologists.

Sláma J, Košler J, Condon D J, et al. 2008. Plesovice zircon – a new natural reference material for U-Pb and Hf isotopic microanalysis. Chemical Geology, 249(1-2): 1-35. doi:10.1016/j.chemgeo.2007.11.005

Spicer R A, Corfield R M. 1992. A review of terrestrial and marine climates in the Cretaceous with implications for modelling the 'Greenhouse Earth'. Geological Magazine, 129(2): 169-180. doi:10.1017/S0016756800008268

Suarez C A, González L A, Ludvigson G A, et al. 2012. Water utilization of the Cretaceous Mussentuchit Member local vertebrate fauna, Cedar Mountain Formation, Utah, USA: using oxygen isotopic composition of phosphate. Palaeogeography, Palaeoclimatology, Palaeoecology, 313: 78-92. doi:10.1016/j.palaeo.2011.10.011

Suarez C A, González L A, Ludvigson G A, et al. 2014. Multi-taxa isotopic investigation of paleohydrology in the Lower Cretaceous Cedar Mountain Formation, eastern Utah, U.S.A.: deciphering effects of the Nevadaplano Plateau on regional climate. Journal of Sedimentary Research, 84: 975-987. doi:10.2110/jsr.2014.76

Suarez M, González L A, Ludvigson G A, et al. 2007. Pedogenic sphaerosiderites from the Caballos Formation (Aptian-Albian) of Columbia; a stable isotope proxy for Cretaceous paleoequatorial precipitation. Geological society of America Abstracts with Programs, 39(3): 75.

Suarez M, González L, Ludvigson G A. 2011. Quantification of a greenhouse hydrologic cycle from equatorial to polar latitudes: the mid-Cretaceous water bearer revisited. Palaeogeography, Palaeoclimatology, Palaeoecology, 307(1): 301-312. doi:10.1016/j.palaeo.2011.05.027

Suarez M, González L A, Ludvigson G A, et al. 2009. Isotopic composition of low-latitude paleoprecipitation during the Early Cretaceous. Geological Society of America Bulletin, 121(11-12): 1584-1595. doi:10.1130/B26453.1

Tera F, Wasserburg G J. 1972. U-Th-Pb systematics in three Apollo 14 basalts and the problem of initial Pb in lunar rocks. Earth and Planetary Science Letters, 14(3): 281-304. doi:10.1016/0012-821X(72)90128-8

Ufnar D F, González L A, Ludvigson G A, et al. 2002. The mid-Cretaceous water bearer: isotope mass balance quantification of the Albian hydrologic cycle. Palaeogeography, Palaeoclimatology, Palaeoecology, 188: 51-71. doi:10.1016/S0031-0182(02)00530-8

Ufnar D F, González L A, Ludvigson G A, et al. 2004. Evidence for increased latent heat transport during the Cretaceous (Albian) greenhouse warming. Geological Society of America, 32(12): 1049-1052. doi:10.1130./G20828.1

Vermeesch P. 2012. On the visualization of detrital age distributions. Chemical Geology, 312: 190-194. Doi:10.1016/j.chemgeo.2012.04.021

Walker J D, Geissman J W, Bowring S A, et al. 2013. The Geological Society of America geologic time scale. Geological Society of America Bulletin, 125(3-4): 259-272. doi:10.1130/B30712.1

Whitmeyer S J, Karlstrom K E. 2007. Tectonic model for the Proterozoic growth of North America. Geosphere, 3(4): 220-259. doi:10.1130/GES00055.1

Wolfe J A, Upchurch G R. 1987. North American nonmarine climates and vegetation during the Late Cretaceous. Palaeogeography, Palaeoclimatology, Palaeoecology, 61: 33-77. doi:10.1016/0031-0182(87)90040-X

Figures

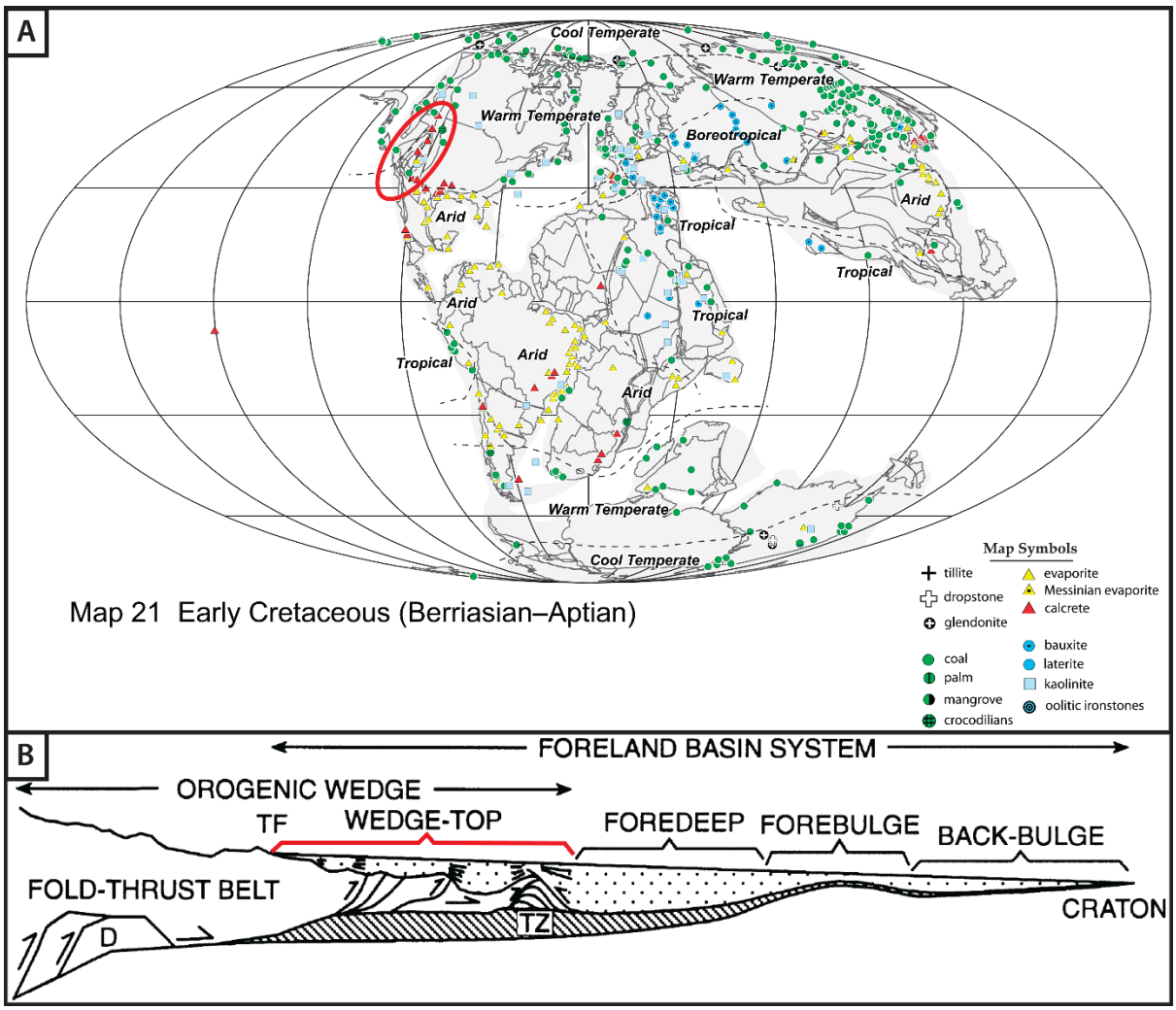

Figure 1. Tectonic and paleoclimatologic setting of the Cretaceous Wayan Formation. A. North-south trending fairway of calcrete deposits in the rain shadow on the leeward (east) site of the Sevier orogen in western North America. This Berriasian-Aptian paleogeographic map from SEPM (Boucot, Xu, & Scotese, 2013) most clearly shows the zonal evaporation deficit of the Hadley Cell in North America to the south of 30° N paleolatitude, and the fairway of calcretes in the rain shadow of the Sevier orogen (in red oval) extending from 30° to 50° N paleolatitude. This paleogeographic map is used by permission by SEPM. Calcretes of the Wayan Formation accumulated in paleosols at 42° N paleolatitude. B. Tectonic setting of the wedge-top depozone (see red bracket) in the foreland basin system, from DeCelles and Giles (1996), used by author's permission.

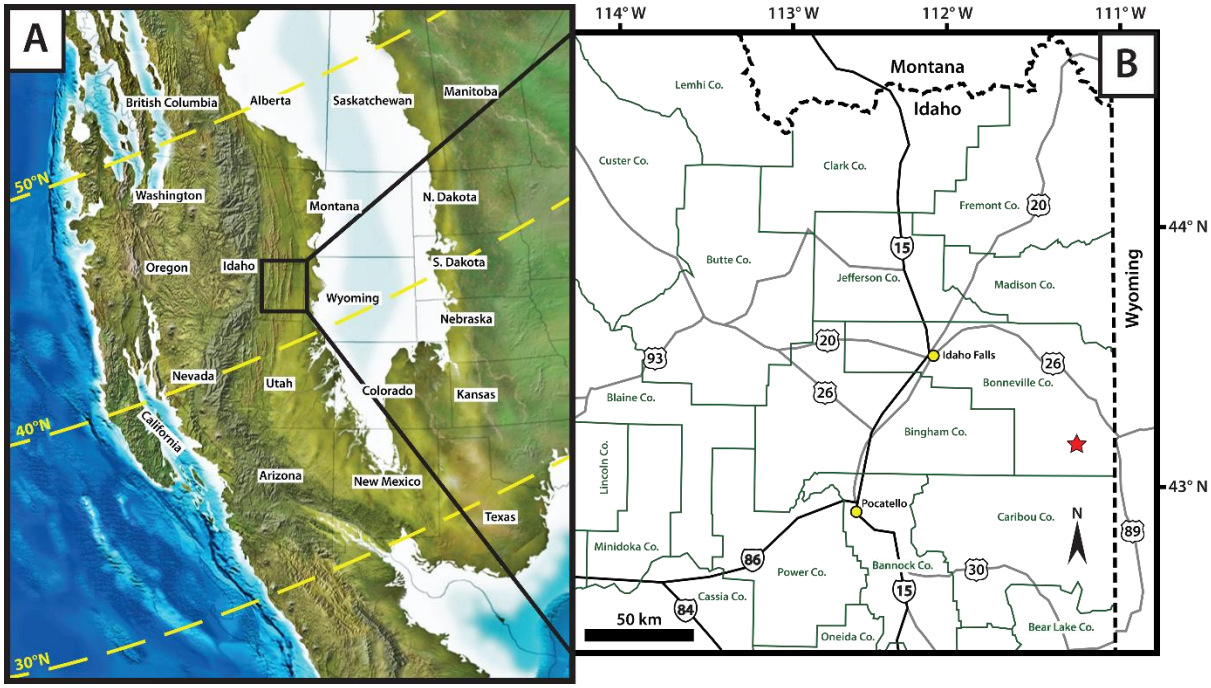

Figure 2. Location of stratigraphic section of Cretaceous Wayan Formation in the Caribou Basin, Bonneville County, Idaho. A. Continental-scale paleogeographic map of North America during the Albian (100 Ma) from (http://cpgeosystems.com/images/WNA_100_KAlb-sm.jpg) ©Ron Blakey, Colorado Plateau Geosystems, used with permission. B. Location of stratigraphic section of the Wayan Formation in the Caribou Basin (red star) in eastern Idaho.

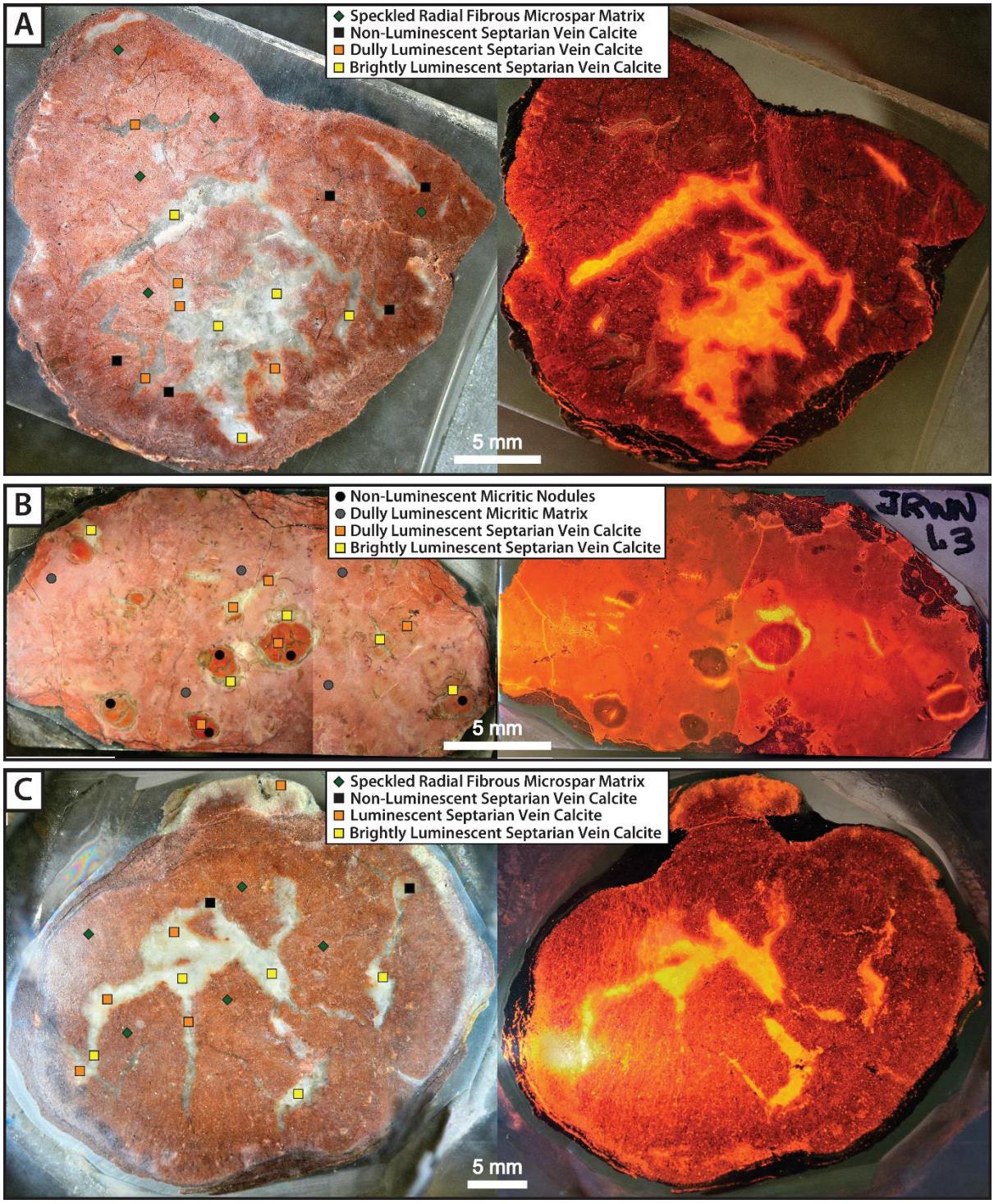

Figure 3. Matching reflected light (left) and cathodoluminescence (right) images of micropolished thick sections slabbed from pedogenic calcite nodules sampled from the Wayan Formation at Caribou Basin, Idaho. Individual calcite components and the locations of microsamples extracted from the thick sections are labelled on the reflected light images, and include CL non-luminescent micritic nodule matrix, CL dully luminescent nodule matrix, CL speckled radial fibrous microspar nodule matrix, CL non-luminescent septarian vein calcite, CL dully luminescent septarian vein calcite, and CL brightly luminescent septarian vein calcite. A. Pedogenic calcite nodule from Wayan 1.2 as shown in Fig. 5. B. Pedogenic calcite nodule from Wayan 1.3 as shown in Fig. 5. C. Pedogenic calcite nodule from Wayan 1.5 as shown in Fig. 5.

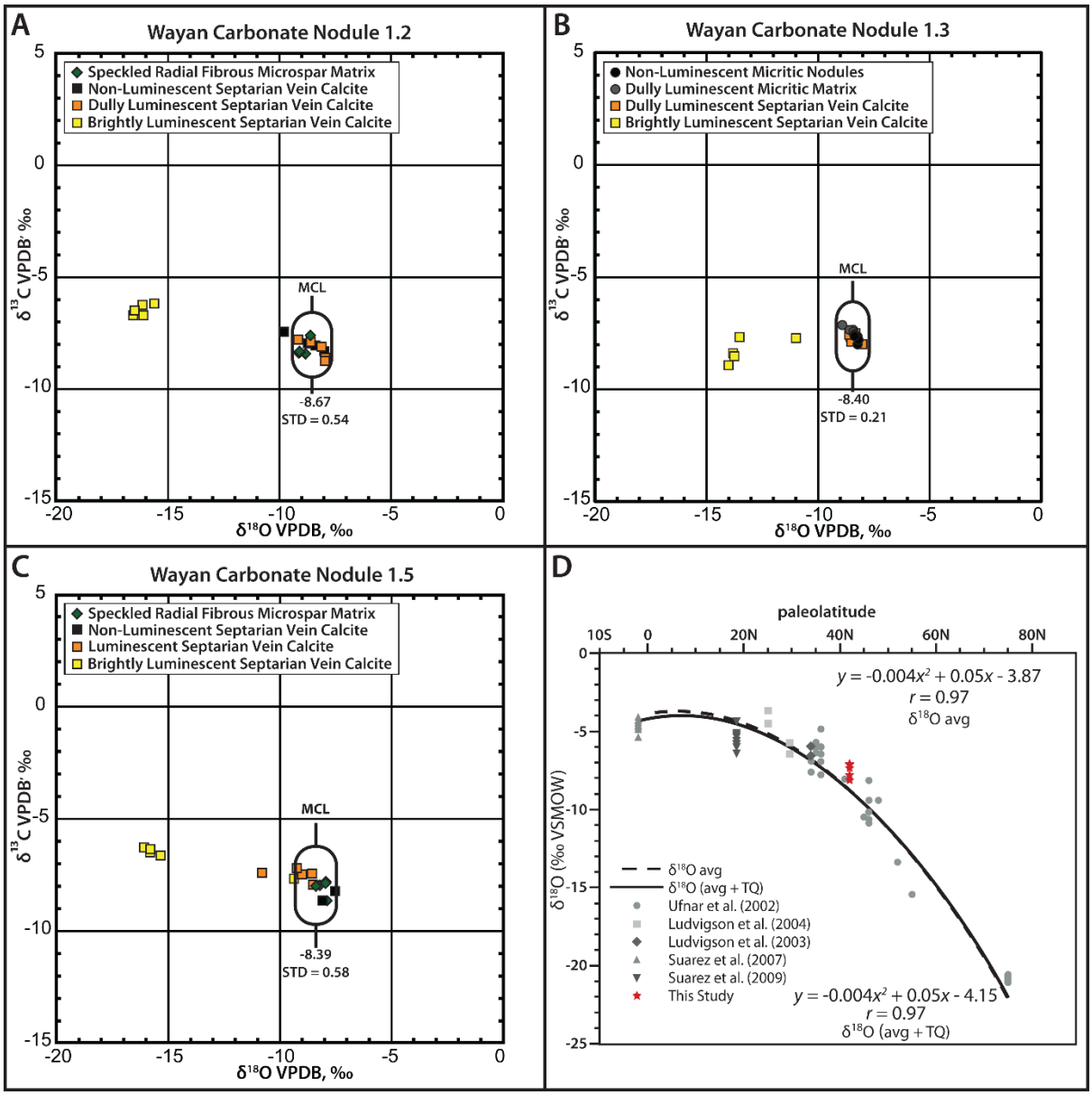

Figure 4. Carbon and oxygen isotope plots of calcite components from pedogenic calcite nodules in the Wayan Formation at Caribou Basin, Idaho. Nodule matrix calcites have relatively invariant $\delta^{18}O$ values conforming to the pattern of meteoric calcite lines (MCLs), with arithmetic means of -8.67, -8.40, and -8.39‰ VPDB, with standard deviations ranging from 0.2 up to 0.58 per mil. Early-formed non-luminescent and dully luminescent vein calcites have carbon and oxygen isotope values that are closely similar to those of the MCL values of the matrix calcites, but the later-formed brightly luminescent septarian vein calcites have much lower $\delta^{18}O$ values ranging from -17 to -11‰ VPDB. A. Carbon and oxygen isotope plot of calcite components from pedogenic calcite nodule Wayan 1.2 as shown in Fig. 5. B. Carbon and oxygen isotope plot of calcite components from pedogenic calcite nodule Wayan 1.3 as shown in Fig. 5. C. Carbon and oxygen isotope plot of calcite components from pedogenic calcite nodule Wayan 1.5 as shown in Fig. 5. D. Cretaceous (Albian) paleolatitudinal transect of the Americas showing calculated groundwater/paleoprecipitation $\delta^{18}O$ values from Suarez et al. (2009; used by author's permission) and the groundwater/paleoprecipitation $\delta^{18}O$ values calculated from MCL values derived from pedogenic carbonates in the Wayan Formation (red stars, this study). The calculated paleoprecipitation values from Wayan Formation at 42° N paleolatitude appear to have a close fit to the polynomial regression of Suarez et al. (2009).

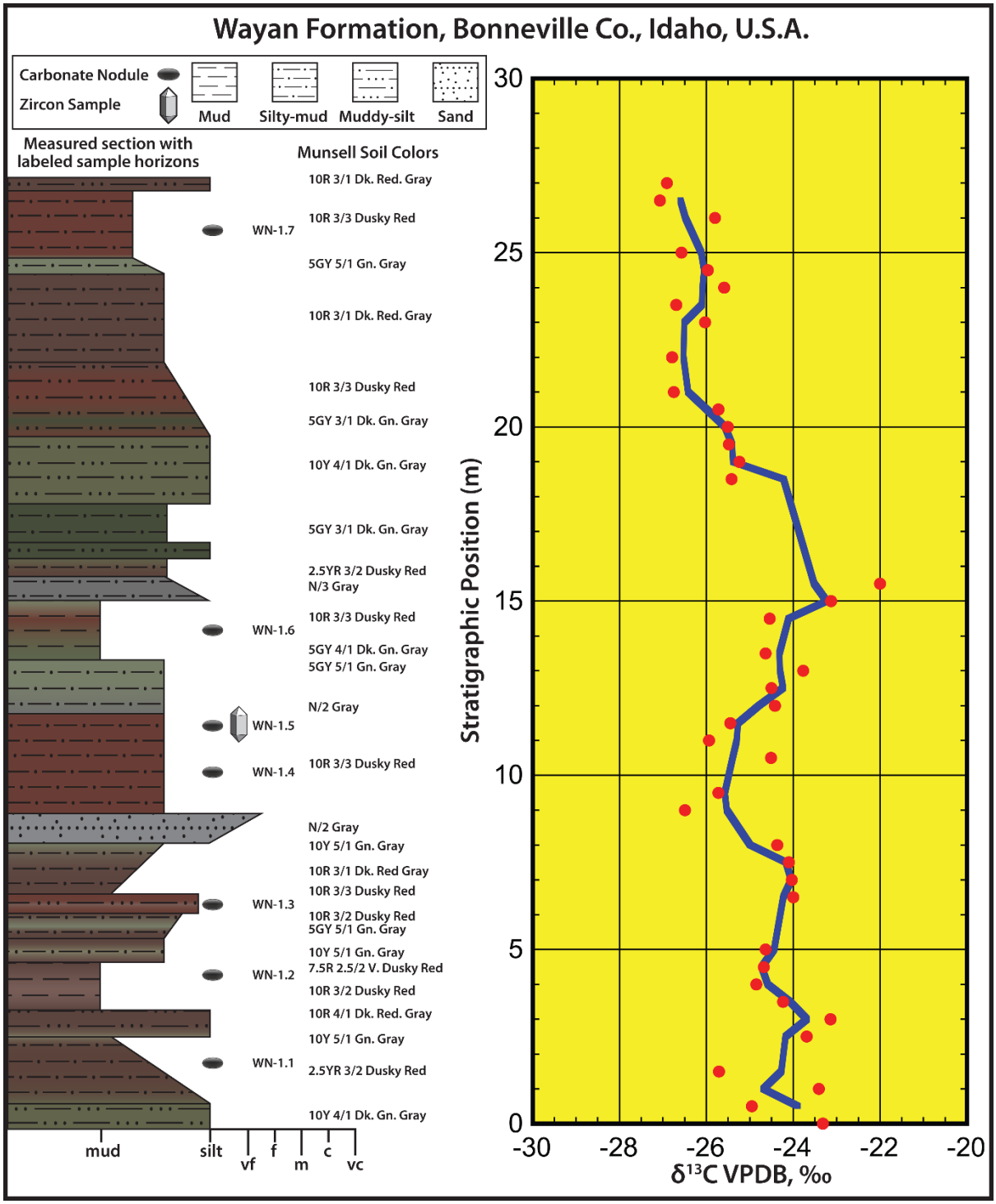

Figure 5. Graphic log and organic carbon chemostratigraphy of exposed 27 meter section of the Wayan Formation at Caribou Basin in Bonneville County, Idaho. To the left, sediment particle sizes ranging from mudstones-siltstones up to fine-grained sandstones are shown in the profile of the graphic log. Munsell soil colors are coded to the right of the graphic log, and are mimicked in the soil colors of the graphic log. Horizontal ellipses and a zircon symbol to the right of the graphic log show the positions of sampled pedogenic carbonates and horizon sampled for U-Pb dating of zircon. To the right, the organic carbon isotope profile shows individual analyses in red dots, along with the three-point moving average in blue line.

Figure 6. Diagrams for the results from U-Pb dating of zircon from sample WN1.5. A. $^{206}Pb/^{238}U$ dates with 2σ

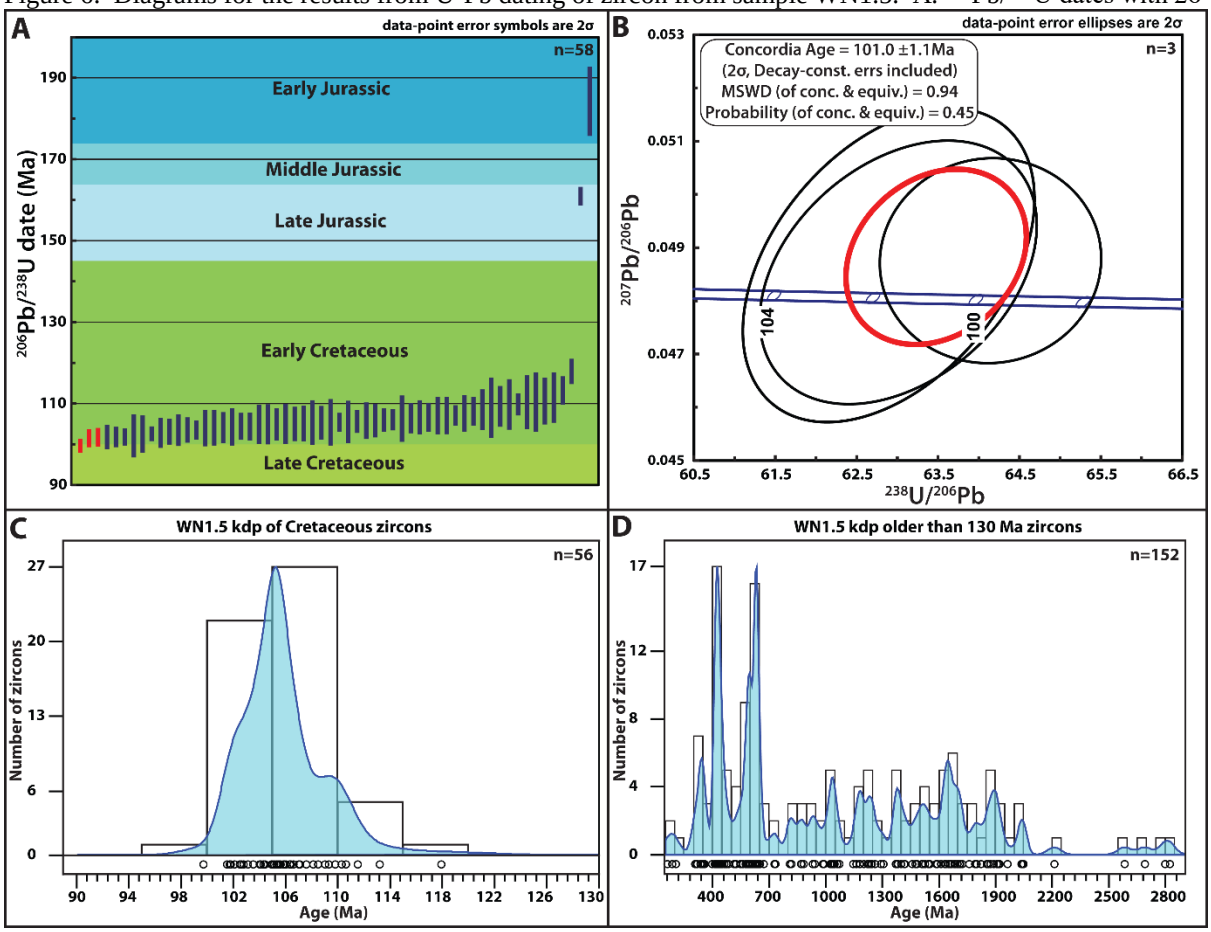

error bars for the 58 youngest analyses, between 90 and 200 Ma, shown on a color-coded geological time scale (Walker et al., 2013). The plot shows a near-continuous range of overlapping dates between ca. 100 Ma and 114 Ma, only 3 grains with dates between 115 Ma and 190 Ma were identified. The three youngest overlapping results (in red) were used to calculate the maximum depositional age (MDA), following the reasoning of Gehrels & Dickinson (2009). B. Tera-Wasserburg concordia diagram (Tera & Wasserburg, 1972) for the three youngest results overlapping within 2σ. The resulting concordia age of 101.0 ± 1.1 Ma is interpreted as the best estimate for the MDA of this sample, placing it near the end of the Albian Age, and thereby the end of the Early Cretaceous Epoch. C and D: Kernel density plots (kdp) for 208 from a total of 209 concordant analyzed grains. C. A kdp for the 58 concordant analyses between ca. 100 and 130 Ma. Plotted are the $^{206}Pb/^{238}U$ dates. D. Kdp for the analyses between 150 and 3000 Ma. Plotted are $^{206}Pb/^{238}U$ dates up to 900 Ma, $^{207}Pb/^{206}Pb$ dates are plotted for older grains. Note the paucity of Jurassic, Triassic and Permian grains.

Figure 7. Aptian-Albian $\delta^{13}C$ chemostratigraphic profiles (left) from Leckie et al. (2002, used with author's

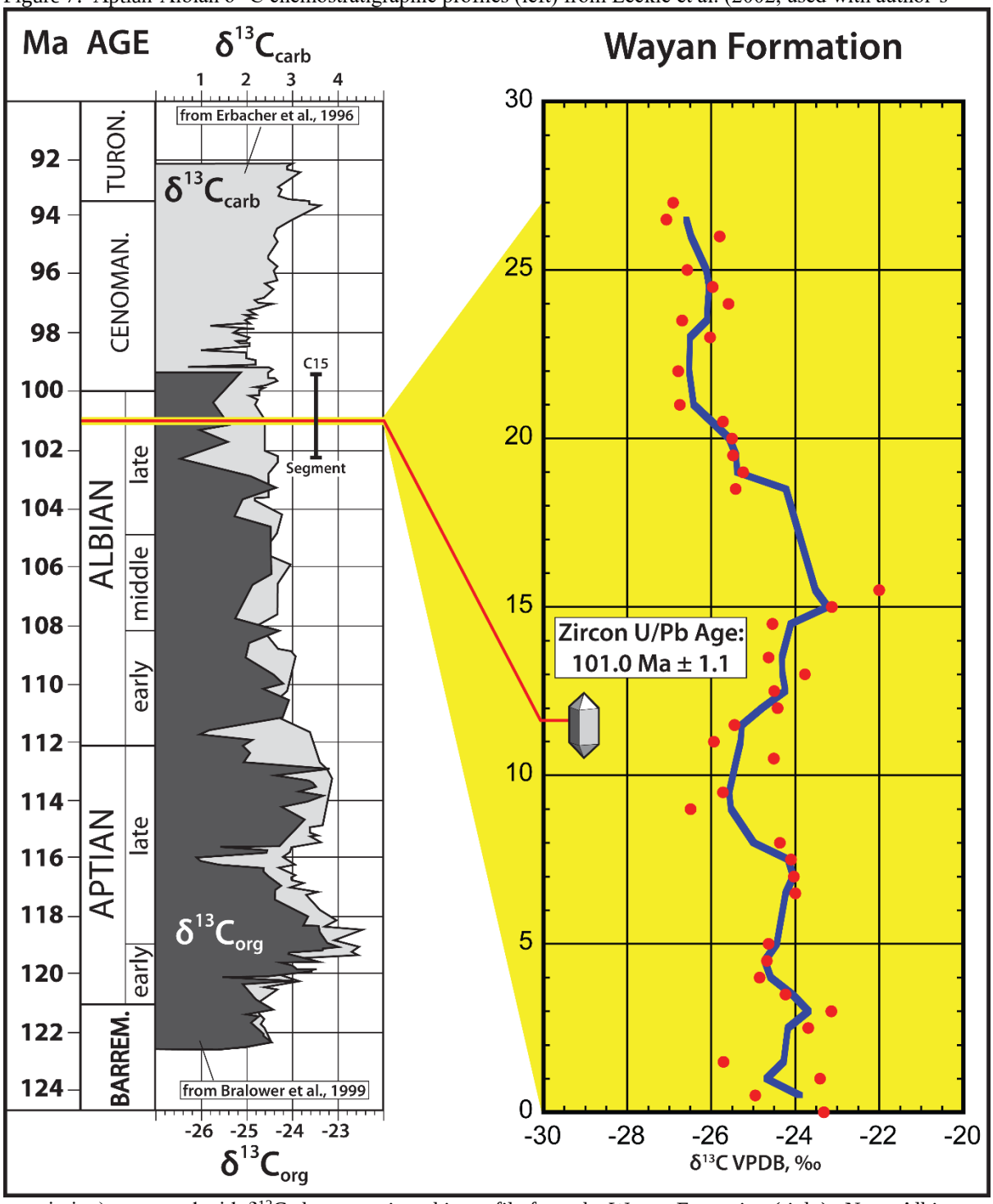

permission) compared with $\delta^{13}C$ chemostratigraphic profile from the Wayan Formation (right). Note: Albian-Cenomanian boundary of Leckie et al. (2002) has been adjusted from 99 Ma to 100 Ma to reflect the Geological Society of America time scale of Walker et al. (2013). U-Pb age of 101.0 ± 1.1 Ma (red line) obtained from zircon sample at 11.6 m interval in the Wayan Formation section correlates to the C15 C-isotope segment reported by Bralower et al. (1999). A distinctive positive $\delta^{13}C$ shift of about 2.5 per mil occurs from 14.5 to 15.5 m levels, followed by a declining trend through the rest of the measured section to a final value -27‰ VPDB.

Appendix A: Zircon Analyses

U-(Th)-Pb geochronological data for zircons from sample WN1.5, sorted from youngest to oldest 206Pb/238U date

Grain #	Signal Duration	Uranium		Thorium		Th/U	equiva-lent U	$^{207}Pb/^{235}U$		$^{206}Pb/^{238}U$		Rho[1]	$^{207}Pb/^{206}Pb$		Age $^{207}Pb/^{235}U$		Age $^{206}Pb/^{238}U$		Age $^{207}Pb/^{206}Pb$		% disc.*	Uncert. wtd. disc,**
	(s)	ppm	2SE	ppm	2SE		ppm	Ratio	Prop2SE	Ratio	Prop2SE		Ratio	Prop2SE	Ma	Prop2SE	Ma	Prop2SE		Prop2SE		
246	9.2	270.7	8.2	89.2	3.5	0.33	292	0.1158	0.0047	0.01558	0.00033	0.1655	0.0541	0.0022	111.8	4.4	99.7	2.1	366	93	10.8	2.8
321	12.7	401	13	239.2	9.8	0.6	457	0.1048	0.0038	0.01559	0.00027	0.4564	0.0479	0.0014	101.1	3.5	99.7	1.7	95	62	1.4	0.4
239	10.9	538	16	150.1	4.3	0.28	573	0.1062	0.0042	0.01587	0.00035	0.1802	0.048	0.0019	102.3	3.8	101.5	2.2	107	79	0.8	0.2
270	11	182.3	5	101.2	4.9	0.56	206	0.1067	0.0048	0.0159	0.00037	0.0537	0.0486	0.0023	102.9	4.4	101.7	2.3	141	96	1.2	0.3
221	12	105.9	4.4	33.8	1.3	0.32	114	0.1088	0.0075	0.01592	0.00047	0.2676	0.0497	0.0033	106.3	7.1	101.8	3	160	130	4.2	0.6
247	12.7	176.9	4.3	53	1.1	0.3	189	0.106	0.0057	0.01592	0.00039	0.2131	0.047	0.0024	102.1	5.2	101.8	2.5	62	99	0.3	0.1
320	12.3	372	30	217	29	0.58	423	0.1091	0.0035	0.01591	0.00033	0.4118	0.0491	0.0015	105.1	3.2	101.8	2.1	150	73	3.1	1
61	12.2	257	11	140.5	5.4	0.55	290	0.1124	0.0076	0.01598	0.00083	0.4158	0.0498	0.0033	107.8	7	102.1	5.3	180	130	5.3	0.8
196	6.6	323	15	94.2	3.6	0.29	345	0.1096	0.0077	0.01604	0.00073	0.2226	0.0508	0.0041	105.4	7.1	102.5	4.6	200	160	2.8	0.4
281	9.1	415	15	194.7	4.3	0.47	461	0.1105	0.0053	0.01604	0.00029	0.1656	0.0503	0.0024	106.3	4.8	102.6	1.8	214	100	3.5	0.8
168	11.4	516	23	122.4	7.2	0.24	545	0.1072	0.0056	0.01607	0.00058	0.519	0.0479	0.0021	103.2	5.2	102.8	3.7	100	88	0.4	0.1
166	12.3	504	31	221	11	0.44	556	0.1075	0.0051	0.01612	0.00051	0.5992	0.0479	0.0018	103.5	4.7	103.1	3.2	102	76	0.4	0.1
174	11.3	965	29	746	28	0.77	1140	0.1145	0.006	0.01619	0.00062	0.6532	0.052	0.0021	109.8	5.5	103.5	3.9	263	87	5.7	1.1
192	12.4	718	41	357	17	0.5	802	0.11	0.0043	0.01619	0.00048	0.4666	0.0493	0.0017	105.8	3.9	103.5	3.1	156	71	2.2	0.6
293	9.9	174	3	60.2	1.3	0.35	188	0.1106	0.0047	0.01618	0.00036	0.1536	0.0483	0.0023	106.4	4.3	103.5	2.3	144	99	2.7	0.7
144	11.7	406	19	177.2	9.2	0.44	448	0.1106	0.0053	0.01626	0.00071	0.4834	0.0496	0.0021	106.4	4.9	104	4.5	166	86	2.3	0.5
132	11.7	183.6	7.7	43.1	1.8	0.23	194	0.106	0.0067	0.01629	0.00069	0.4778	0.0481	0.0026	102	6.2	104.1	4.4	110	110	-2.1	-0.3
162	11.6	416	28	166.7	8.3	0.4	455	0.1084	0.0056	0.01629	0.00059	0.4874	0.0479	0.0021	104.3	5.1	104.1	3.8	101	86	0.2	0
88	11	539	28	238	15	0.44	595	0.1095	0.006	0.01632	0.00072	0.553	0.0487	0.0023	105.4	5.5	104.3	4.6	144	99	1	0.2
208	12	364	13	181.1	4.2	0.5	407	0.1061	0.0038	0.01633	0.00053	0.1873	0.0469	0.002	102.3	3.5	104.4	3.3	59	83	-2.1	-0.6
220	11.3	165.2	6.1	42.3	1.5	0.26	175	0.1072	0.0061	0.01634	0.00054	0.3159	0.0479	0.0025	103.9	5.7	104.4	3.4	100	100	-0.5	-0.1
127	12.3	233	22	79.6	7.8	0.34	252	0.1082	0.0071	0.01642	0.00075	0.4771	0.0478	0.0027	103.9	6.5	104.9	4.8	100	110	-1	-0.2
151	7.4	211	14	52	2.6	0.25	223	0.1075	0.0065	0.01641	0.00077	0.2636	0.0497	0.0034	103.5	6	104.9	4.9	170	140	-1.4	-0.2
154	12.6	487	20	167.1	4.5	0.34	526	0.1102	0.0053	0.0164	0.00063	0.5387	0.0497	0.0021	106	4.9	104.9	4	174	87	1	0.2
116	11.3	146.4	6	58.8	2.2	0.4	160	0.1056	0.0082	0.01643	0.00077	0.4082	0.0476	0.0035	101.5	7.5	105	4.9	100	140	-3.4	-0.5
128	12.4	271	16	95.2	4.6	0.35	293	0.1043	0.0056	0.01643	0.00066	0.4014	0.0468	0.0026	100.5	5.2	105	4.2	60	110	-4.5	-0.9
171	8.9	332	28	105	10	0.32	357	0.1157	0.0075	0.01644	0.0007	0.409	0.05	0.0025	110.9	6.8	105.1	4.4	190	100	5.2	0.9
72	12.2	265	15	99	6.6	0.37	288	0.1075	0.0067	0.01647	0.00087	0.3864	0.0482	0.0033	103.4	6.1	105.3	5.5	100	130	-1.8	-0.3
155	11.5	515	22	215	21	0.42	566	0.112	0.0046	0.01647	0.00064	0.5188	0.0497	0.0022	107.7	4.2	105.3	4.1	175	92	2.2	0.6
145	5.5	304	13	97.9	6.2	0.32	327	0.1102	0.0069	0.01649	0.0009	0.1852	0.0487	0.0034	106	6.3	105.4	5.7	160	150	0.6	0.1

Grain #	Signal Duration	Uranium		Thorium		Th/U	equiva-lent U	$^{207}Pb/^{235}U$		$^{206}Pb/^{238}U$		Rho[1]	$^{207}Pb/^{206}Pb$		Age $^{207}Pb/^{235}U$		Age $^{206}Pb/^{238}U$		Age $^{207}Pb/^{206}Pb$		% disc.*	Uncert. wtd. disc,**
	(s)	ppm	2SE	ppm	2SE		ppm	Ratio	Prop2SE	Ratio	Prop2SE		Ratio	Prop2SE	Ma	Prop2SE	Ma	Prop2SE		Prop2SE		
305	12.5	279	13	98	10	0.35	302	0.1102	0.0042	0.01649	0.00037	0.1334	0.0472	0.0018	106	3.9	105.4	2.3	82	79	0.6	0.2
74	12.2	381	21	171	17	0.45	421	0.1103	0.007	0.0165	0.00081	0.4635	0.0485	0.0029	105.9	6.3	105.5	5.2	130	120	0.4	0.1
240	113	96	4	31	1.2	0.32	103	0.1094	0.0078	0.01653	0.00045	0.4	0.0483	0.0036	106.1	6.9	105.6	2.8	130	150	0.5	0.1
142	117	314	17	80.2	3	0.26	333	0.1099	0.0069	0.01655	0.00071	0.3739	0.0487	0.0027	107.3	6.3	105.8	4.5	140	110	1.4	0.2
159	12.3	285	11	123.3	4.9	0.43	314	0.1109	0.0066	0.01646	0.00064	0.5145	0.0498	0.0025	106.5	6	105.8	4.1	169	100	0.7	0.1
218	12.2	193.4	6.6	81	2.4	0.42	212	0.1075	0.0057	0.01656	0.00045	0.2652	0.0483	0.0024	103.5	5.2	105.9	2.9	117	98	-2.3	-0.5
227	115	942	32	507	24	0.54	1061	0.1087	0.0037	0.01658	0.00041	0.5369	0.0477	0.0014	104.7	3.3	106	2.6	91	62	-1.2	-0.4
4	12.4	217	16	66.5	4	0.31	233	0.1108	0.0065	0.01663	0.0009	0.4596	0.0476	0.0028	106.4	5.9	106.3	5.7	80	110	0.1	0
157	116	477	24	207.4	8.5	0.43	526	0.1092	0.0057	0.01664	0.00058	0.5356	0.0481	0.0021	105.1	5.2	106.4	3.7	119	89	-1.2	-0.3
147	12.4	416	19	180.5	7.3	0.43	458	0.1122	0.0055	0.01659	0.00064	0.4367	0.0482	0.0022	107.8	5	106.6	4.2	147	97	1.1	0.2
148	12.2	231	11	63.9	2.2	0.28	246	0.1092	0.0062	0.01667	0.00056	0.3681	0.0488	0.0026	105	5.7	106.6	3.6	150	110	-1.5	-0.3
115	118	471	17	202.2	7.5	0.43	519	0.1157	0.0073	0.01673	0.00072	0.5658	0.0502	0.0025	111.7	6.7	107	4.6	190	100	4.2	0.7
203	113	177	11	104.5	6.9	0.59	202	0.0981	0.0061	0.01673	0.00054	0.41	0.0434	0.0025	95.6	5.8	107	3.4	-86	99	-11.9	-2
79	12.2	94.4	6.2	33.4	1.7	0.35	102	0.109	0.01	0.01675	0.00072	0.3984	0.0459	0.0037	104.3	9.1	107.1	4.6	30	150	-2.7	-0.3
229	114	229	13	101.1	5.1	0.44	253	0.1109	0.0047	0.01675	0.00039	0.277	0.0485	0.0021	106.7	4.3	107.1	2.5	127	86	-0.4	-0.1
120	119	270.8	9.4	178	13	0.66	313	0.1078	0.0071	0.01683	0.00071	0.4959	0.0481	0.0026	103.6	6.5	107.6	4.5	100	100	-3.9	-0.6
231	8.2	284	17	169.1	5.2	0.6	324	0.1155	0.0059	0.01692	0.00055	0.4256	0.0496	0.0022	110.8	5.4	108.1	3.5	186	94	2.4	0.5
91	12.4	269	37	69.5	7.5	0.26	285	0.1138	0.0081	0.01698	0.00078	0.4939	0.0489	0.0029	109	7.4	108.5	5	130	110	0.5	0.1
14	114	106.4	6.1	24.5	1.2	0.23	112	0.111	0.011	0.0171	0.0012	0.4164	0.0456	0.004	106	10	109	7.4	50	170	-2.8	-0.3
130	6.7	467	20	183.8	8.9	0.39	510	0.1151	0.0073	0.01711	0.00079	0.7109	0.0492	0.0023	110.4	6.7	109.3	5	176	100	1	0.2
6	119	304	46	36.1	3.1	0.12	312	0.1071	0.0071	0.01719	0.00098	0.5492	0.0459	0.0026	103.8	6.3	109.8	6.2	20	110	-5.8	-1
242	10.8	168	5.5	36.6	1.8	0.22	177	0.115	0.0061	0.01718	0.00043	0.4	0.0492	0.003	110.3	5.5	109.8	2.7	160	120	0.5	0.1
9	10.8	577	34	186	11	0.32	621	0.114	0.01	0.0173	0.001	0.4275	0.0474	0.0036	109.2	9.2	110.3	6.6	70	140	-1	-0.1
20	119	259	20	53.9	3.3	0.21	272	0.115	0.01	0.0173	0.0012	0.5787	0.0497	0.0038	111.2	9.3	110.3	7.3	170	150	0.8	0.1
64	12.2	158.5	7.5	109.3	3.7	0.69	184	0.1157	0.0091	0.01731	0.00089	0.3267	0.0487	0.0036	110.6	8.3	110.6	5.7	140	140	0	0
30	12.5	305	22	93.9	4.4	0.31	327	0.12	0.011	0.01746	0.00097	0.594	0.05	0.0039	114	10	111.5	6.2	220	150	2.2	0.3
201	8.8	291	32	113	16	0.39	318	0.1176	0.0065	0.01772	0.00055	0.3331	0.0493	0.0027	112.7	6	113.2	3.5	160	110	-0.4	-0.1
254	5.5	726	26	372	16	0.51	813	0.1245	0.0046	0.01845	0.00049	0.5338	0.0488	0.0015	119.1	4.1	117.9	3.1	150	69	1	0.3
183	9.2	653	18	694	23	1.06	816	0.463	0.019	0.01872	0.00064	0.5438	0.1795	0.0067	386	13	119.5	4.1	2633	61	69	20.5
308	117	331	15	118.4	7.6	0.36	359	0.1751	0.0052	0.02528	0.00037	0.2437	0.0496	0.0015	163.7	4.5	160.9	2.3	171	64	17	0.6

Grain #	Signal Duration	Uranium		Thorium		Th/U	equiva-lent U	$^{207}Pb/^{235}U$		$^{206}Pb/^{238}U$		Rho[1]	$^{207}Pb/^{206}Pb$		Age $^{207}Pb/^{235}U$		Age $^{206}Pb/^{238}U$		Age $^{207}Pb/^{206}Pb$		% disc.*	Uncert. wtd. disc,**
	(s)	ppm	2SE	ppm	2SE		ppm	Ratio	Prop2SE	Ratio	Prop2SE		Ratio	Prop2SE	Ma	Prop2SE	Ma	Prop2SE		Prop2SE		
214	4.2	76.1	3.1	60.0	2.6	0.79	90.2	0.202	0.012	0.029	0.0014	0.5406	0.0507	0.002	186.6	10	184.2	8.5	219	89	1.3	0.2
173	11.8	207.8	8.6	78.1	2.7	0.38	22.6	0.22	0.011	0.0323	0.0011	0.4423	0.0493	0.0022	201.3	9.3	205	7.1	155	91	-1.8	-0.4
178	11.8	148.2	3.8	39.5	1.5	0.27	157.5	0.364	0.015	0.0452	0.0014	0.591	0.0587	0.0021	316	11	284.6	8.7	541	75	9.9	2.9
276	11.8	29.2	1.1	28.8	1.2	0.99	36.0	0.475	0.056	0.04863	0.00091	0.6368	0.0719	0.008	385	35	306.1	5.6	890	200	20.5	2.3
135	11.8	44.7	1.5	39.1	1.4	0.87	54	0.355	0.024	0.0489	0.0024	0.2512	0.0552	0.0043	308	18	307	15	360	150	0.3	0.1
63	11.8	63.6	3.2	77	3.5	0.12	65.4	0.363	0.027	0.0492	0.0027	0.6301	0.0537	0.0035	311	20	309	16	340	140	0.6	0.1
55	11.8	26.3	1.3	157.8	8.7	0.6	30.0	0.373	0.028	0.0505	0.0029	0.505	0.0548	0.0041	322	21	317	18	370	150	1.6	0.2
317	11.8	74.2	8.4	94.0	12.0	1.27	96.3	0.956	0.055	0.0511	0.0015	0.6416	0.1335	0.0054	682	29	321	9.5	2140	72	52.9	12.4
78	11.8	47.2	4.9	22.5	1.3	0.48	52.5	0.471	0.029	0.0524	0.0024	0.2957	0.0664	0.0042	392	21	329	15	740	130	16.1	3
85	11.8	91.6	4.5	65.6	2.3	0.72	107.0	0.425	0.03	0.0529	0.003	0.5715	0.0589	0.0034	356	22	334	19	500	120	6.2	1
122	11.8	133.5	6.6	37.6	1.5	0.28	14.2	0.403	0.021	0.0547	0.0018	0.4619	0.0545	0.0027	344	15	343	11	370	110	0.3	0.1
205	11.8	47.3	1.4	212.4	4.7	0.45	52.3	0.415	0.013	0.0547	0.0017	0.4748	0.0542	0.0018	351.6	9.5	343	10	369	74	2.4	0.9
323	11.8	271.6	6	83.7	1.8	0.31	29.1	0.4082	0.0095	0.05538	0.00066	0.2156	0.0533	0.0013	347.3	6.8	347.4	4	332	54	0	0
45	11.8	103.5	8.8	88.8	9.7	0.09	105.6	0.553	0.044	0.0558	0.0032	0.5426	0.0724	0.005	440	29	349	19	920	140	20.7	3.1
327	11.8	173.1	5.4	61.1	3	0.35	18.7	0.423	0.012	0.05619	0.00071	0.1688	0.0542	0.0015	358.8	8.1	352.4	4.3	373	63	1.8	0.8
3	11.6	80.3	6.2	33.8	4.8	0.04	81.1	0.438	0.023	0.0572	0.0029	0.5283	0.0556	0.0027	367	16	358	18	420	100	2.5	0.6
40	11.8	96.0	15.0	79.0	13.0	0.82	114.6	0.861	0.082	0.0576	0.004	0.1591	0.11	0.012	616	44	360	24	1730	200	41.6	5.8
256	11.8	68.1	3.3	35.0	3.8	0.51	76.3	0.593	0.03	0.0578	0.0014	0.5561	0.0736	0.0041	476	19	362.2	8.3	1010	120	23.9	6
77	11.8	171.0	15.0	24.7	1.5	0.14	176.8	1.08	0.052	0.0615	0.0027	0.64	0.1275	0.0049	742	25	384	16	2052	65	48.2	14.3
202	11.8	76.1	8.0	51.8	4.2	0.07	77.3	0.498	0.018	0.0634	0.0018	0.6207	0.0573	0.0016	409	12	396	11	495	61	3.2	1.1
199	11.8	30.8	5.2	12.1	1.6	0.39	33.6	0.697	0.031	0.0645	0.0023	0.1182	0.0792	0.0042	534	18	403	14	1180	110	24.5	7.3
283	11.8	66.6	7.0	10.0	1.5	0.15	69.0	0.504	0.011	0.0656	0.001	0.4783	0.0557	0.0012	414.1	7.4	409.8	6.1	435	50	1	0.6
291	11.8	73.2	1.6	7.61	0.94	0.01	73.4	0.5053	0.011	0.0657	0.001	0.4819	0.0557	0.0011	415	7.1	410.4	6.1	437	44	1.1	0.6
258	11.8	78.4	5.7	2.3	0.47	0.03	79	0.504	0.02	0.0662	0.0017	0.4561	0.0551	0.002	413	13	413	10	392	78	0	0
46	11.8	65.1	6.3	131.2	8.2	0.2	68.2	0.501	0.039	0.0666	0.0041	0.5279	0.0561	0.0038	411	27	415	25	410	140	-1	-0.1
253	11.8	25.5	1.2	85.3	3.1	0.33	27.5	0.507	0.014	0.067	0.0012	0.4554	0.0548	0.0013	417.1	9.4	418.2	7.3	393	55	-0.3	-0.1
206	11.8	17.0	1.8	20.01	0.9	0.12	17.5	0.506	0.02	0.0674	0.0021	0.4934	0.0552	0.0022	416	14	420	13	395	85	-1	-0.3
295	11.8	54.9	1.5	211.2	5.7	0.38	59.9	0.5207	0.0099	0.06735	0.00087	0.4749	0.0565	0.001	425.4	6.6	420.1	5.3	466	40	1.2	0.8
294	11.8	98.0	4.6	42.0	1.7	0.43	107.9	0.597	0.02	0.0677	0.0013	0.4152	0.0631	0.0019	474	13	422.2	7.8	695	62	10.9	4
66	11.8	153.8	8.2	114.1	3.8	0.74	18.1	0.52	0.033	0.0678	0.0032	0.517	0.0561	0.003	425	22	423	19	430	120	0.5	0.1

Grain #	Signal Duration	Uranium		Thorium		Th/U	equiva-lent U	$^{207}Pb/^{235}U$		$^{206}Pb/^{238}U$		Rho[1]	$^{207}Pb/^{206}Pb$		Age $^{207}Pb/^{235}U$		Age $^{206}Pb/^{238}U$		Age $^{207}Pb/^{206}Pb$		% disc.*	Uncert. wtd. disc,**
	(s)	ppm	2SE	ppm	2SE		ppm	Ratio	Prop2SE	Ratio	Prop2SE		Ratio	Prop2SE	Ma	Prop2SE	Ma	Prop2SE		Prop2SE		
121	118	184.7	8.8	23.14	0.74	0.13	190	0.523	0.029	0.0684	0.0025	0.463	0.0564	0.0028	424	19	426	15	420	110	-0.5	-0.1
65	118	154.3	7.8	36.5	1.5	0.24	163	0.581	0.043	0.0686	0.0034	0.3073	0.062	0.004	459	27	427	21	590	130	7	1.2
156	118	207.3	9.6	137.4	7	0.66	240	0.523	0.026	0.0687	0.0027	0.5805	0.0559	0.0024	427	18	428	17	413	94	-0.2	-0.1
23	118	94.4	9.8	20.9	1.2	0.22	99	0.517	0.047	0.0691	0.0045	0.5484	0.0571	0.0048	420	32	430	27	420	170	-2.4	-0.3
138	118	241	14	74.6	6.1	0.31	259	0.528	0.026	0.07	0.0029	0.544	0.0563	0.0025	428	17	436	17	429	98	-1.9	-0.5
257	118	617	14	213	17	0.35	667	0.666	0.018	0.0708	0.0014	0.4966	0.0675	0.0016	519	11	440.6	8.4	856	48	15.1	7.1
180	118	533	25	261.1	8.2	0.49	594	0.538	0.021	0.0706	0.0025	0.5844	0.0564	0.0019	438	14	441	15	447	73	-0.7	-0.2
285	118	234	25	64.8	7.8	0.28	249	0.661	0.091	0.0714	0.009	0.9823	0.0673	0.0018	525	56	441	53	856	53	16	1.5
245	118	161	11	102.3	7.1	0.64	185	0.56	0.021	0.0712	0.0016	0.4966	0.0575	0.0018	452	13	443.2	9.7	488	69	1.9	0.7
129	118	123	10	70.2	4.1	0.57	139	0.54	0.024	0.0714	0.0027	0.4503	0.0558	0.0026	447	16	444	16	406	100	0.7	0.2
259	118	216	22	79	13	0.37	235	0.528	0.021	0.0713	0.0022	0.7746	0.0548	0.0015	431	14	444	13	404	61	-3	-0.9
193	118	105.9	4.6	37.91	0.84	0.36	115	0.542	0.023	0.0723	0.0027	0.6282	0.0544	0.0018	438	15	450	16	375	76	-2.7	-0.8
16	118	267	14	7.79	0.59	0.03	269	0.574	0.045	0.0744	0.0048	0.5934	0.0567	0.0037	462	30	461	29	450	140	0.2	0
37	118	826	54	537	28	0.65	952	0.702	0.064	0.0744	0.0048	0.591	0.073	0.0059	529	37	462	29	940	170	12.7	1.8
56	118	491	25	205	14	0.42	539	0.668	0.053	0.0745	0.0043	0.514	0.0655	0.0043	511	32	462	26	700	140	9.6	1.5
177	118	233.3	8.4	73.1	3.2	0.31	250	0.614	0.034	0.0744	0.0029	0.6874	0.0593	0.0023	483	22	462	17	544	84	4.3	1
52	118	252	14	158.6	6.6	0.63	289	0.687	0.042	0.0755	0.0038	0.5932	0.0685	0.0036	529	26	468	23	850	110	11.5	2.3
82	118	319	17	155	6.1	0.49	355	0.589	0.037	0.0762	0.0039	0.5936	0.0577	0.0031	466	23	473	24	500	120	-1.5	-0.3
280	118	761	42	1215	5.4	0.16	790	0.989	0.039	0.0765	0.0015	0.4	0.0935	0.0039	698	20	476	8.9	1519	84	31.8	11.1
260	118	137	14	73.2	6.6	0.53	154	0.99	0.16	0.0769	0.0024	0.7847	0.09	0.011	679	73	477	14	1320	230	29.7	2.8
24	118	529	50	127	12	0.24	559	0.661	0.06	0.0783	0.0052	0.5823	0.0612	0.0049	504	37	485	31	550	170	3.8	0.5
44	118	504	45	465	37	0.92	613	2	1.2	0.081	0.012	0.9289	0.119	0.027	690	110	499	67	1420	290	27.7	1.7
5	118	189	15	66.8	4.4	0.35	205	0.648	0.04	0.0822	0.0047	0.6327	0.0567	0.0029	506	25	512	27	460	110	-1.2	-0.2
134	118	358	14	38.1	3.3	0.11	367	0.727	0.038	0.0836	0.0035	0.49	0.0634	0.0028	551	22	517	21	691	97	6.2	1.5
136	118	480	15	299	24	0.62	550	0.697	0.033	0.0845	0.0029	0.4925	0.0589	0.0025	537	19	523	17	562	92	2.6	0.7
303	118	234.3	8.1	14.81	0.47	0.06	238	0.718	0.019	0.0883	0.0012	0.3896	0.0589	0.0015	549	11	546.3	7.6	557	56	0.5	0.2
325	118	86.3	2.9	47.1	1.3	0.55	97	0.726	0.023	0.089	0.0012	0.1215	0.0584	0.0019	553	14	549.3	6.9	521	73	0.7	0.3
1	8.2	259.5	6.7	115	3.8	0.44	287	0.738	0.024	0.0907	0.0036	0.7075	0.0588	0.0017	560	14	560	21	546	63	0	0
57	118	60.8	3.7	39.3	1.6	0.65	70	0.749	0.059	0.0934	0.005	0.4587	0.0592	0.0041	563	34	575	30	550	150	-2.1	-0.4
282	118	47.8	2	45.99	0.94	0.96	59	0.799	0.032	0.0934	0.0021	0.4275	0.0623	0.0021	599	19	578	12	692	76	3.5	1.1

Grain #	Signal Duration	Uranium		Thorium		Th/U	equiva-lent U	$^{207}Pb/^{235}U$		$^{206}Pb/^{238}U$		Rho[1]	$^{207}Pb/^{206}Pb$		Age $^{207}Pb/^{235}U$		Age $^{206}Pb/^{238}U$		Age $^{207}Pb/^{206}Pb$		% disc.*	Uncert. wtd. disc,**
	(s)	ppm	2SE	ppm	2SE		ppm	Ratio	Prop2SE	Ratio	Prop2SE		Ratio	Prop2SE	Ma	Prop2SE	Ma	Prop2SE		Prop2SE		
13	118	114.9	4.8	22.5	1.4	0.2	120	0.799	0.052	0.0952	0.0056	0.5538	0.0614	0.0033	589	30	585	33	640	120	0.7	0.1
96	118	214	12	12.41	0.61	0.58	24	0.839	0.064	0.0953	0.0049	0.4286	0.0624	0.0042	613	34	586	29	670	150	4.4	0.8
298	118	89.7	3.6	40.7	1.3	0.45	99	0.769	0.021	0.0959	0.0017	0.1274	0.0587	0.0017	578	12	590.2	9.9	546	62	-2.1	-1
228	118	618	17	17.07	0.34	0.28	66	0.802	0.026	0.0968	0.0026	0.3065	0.0615	0.0024	597	15	595	15	646	85	0.3	0.1
269	118	328.5	9.5	164.8	3.2	0.5	367	0.824	0.02	0.0968	0.0015	0.4506	0.0619	0.0012	609	11	595.7	8.6	681	47	2.2	1.2
324	118	189.4	6.1	69.2	1.7	0.37	206	0.813	0.022	0.0969	0.0012	0.4705	0.0601	0.0014	605	12	595.9	7.2	615	50	1.5	0.8
67	118	161.1	8.2	53.3	2	0.33	174	0.786	0.049	0.0976	0.005	0.5179	0.0609	0.0034	591	29	600	30	590	120	-1.5	-0.3
124	118	228	10	116.5	5.5	0.51	255	0.851	0.043	0.0993	0.0046	0.5966	0.0616	0.0027	624	23	609	27	618	98	2.4	0.7
114	118	421	18	152	13	0.36	457	0.833	0.044	0.0995	0.0044	0.6178	0.0617	0.0027	620	26	611	26	622	96	1.5	0.3
176	118	502	22	76.6	2.7	0.15	520	0.81	0.034	0.1	0.0034	0.5519	0.0599	0.0022	604	19	614	20	582	80	-1.7	-0.5
272	118	34.1	2.4	22.23	0.68	0.65	39	0.911	0.037	0.1005	0.0025	0.2657	0.0644	0.0027	655	20	619	15	746	91	5.5	1.8
150	118	515	84	125.3	7	0.24	544	1.247	0.061	0.1006	0.0042	0.5315	0.092	0.004	823	28	621	25	1452	85	24.5	7.2
328	118	444	10	26.88	0.82	0.06	450	0.854	0.019	0.1016	0.0012	0.626	0.0606	0.0011	628.8	11	623.5	6.9	618	41	0.8	0.5
274	118	230	11	141	10	0.61	263	0.847	0.02	0.102	0.0016	0.5721	0.0606	0.0012	623.4	11	626	9.3	618	43	-0.4	-0.2
197	118	602	16	357	11	0.59	686	0.847	0.027	0.1023	0.0028	0.6831	0.0615	0.0016	627	16	627	16	663	57	0	0
312	118	52.6	1.9	57.4	1.6	1.09	66	0.868	0.034	0.1023	0.0016	0.1555	0.0609	0.0024	632	19	627.5	9.2	640	81	0.7	0.2
15	118	148	16	80.3	4.4	0.54	167	0.893	0.078	0.1034	0.0067	0.5609	0.0632	0.0048	640	42	632	39	630	160	1.3	0.2
87	118	375	16	519	20	1.38	497	0.876	0.05	0.1032	0.0051	0.6243	0.0617	0.0028	637	27	632	30	640	100	0.8	0.2
53	118	225	19	150	13	0.67	260	0.903	0.063	0.1037	0.0054	0.6189	0.0634	0.0039	657	34	635	32	690	130	3.3	0.6
289	118	370	26	122.3	7.3	0.33	399	0.862	0.018	0.1036	0.0017	0.525	0.0602	0.0012	632	10	635.3	9.7	604	44	-0.5	-0.3
175	118	400	14	121.6	3.2	0.3	429	0.94	0.033	0.1039	0.0033	0.503	0.0654	0.0023	671	17	636	20	779	77	5.2	2.1
59	118	385	27	108.9	7.5	0.28	411	0.877	0.058	0.1041	0.0056	0.5977	0.0622	0.0037	636	32	637	33	640	130	-0.2	0
60	118	627	28	22.47	0.78	0.04	632	0.904	0.061	0.1042	0.0054	0.5071	0.0642	0.0038	650	32	638	31	690	130	1.8	0.4
80	118	392	18	193.5	6.3	0.49	437	0.873	0.05	0.1043	0.0051	0.5454	0.0612	0.0032	638	26	638	30	630	110	0	0
223	118	241.9	7.8	72.8	4.9	0.3	259	0.876	0.036	0.106	0.0035	0.754	0.0605	0.0018	639	19	649	21	623	62	-1.6	-0.5
266	118	141.6	7.6	52.5	1.1	0.37	154	0.894	0.026	0.1061	0.0022	0.6997	0.0608	0.0013	649	14	650	13	631	46	-0.2	-0.1
273	118	131	8.3	99	8.7	0.76	154	0.874	0.025	0.106	0.0018	0.5073	0.0597	0.0015	636	13	650	11	595	52	-2.2	-1.1
234	118	86.4	3.1	30.7	0.89	0.36	94	0.934	0.03	0.1098	0.0028	0.5248	0.0618	0.0017	668	16	671	16	662	59	-0.4	-0.2
32	118	255	16	71.4	4.9	0.28	272	3.2	1.2	0.115	0.012	0.935	0.152	0.039	1040	180	697	69	1650	360	33	1.9
210	118	448	12	81.7	6.1	0.18	467	1.335	0.099	0.1193	0.007	0.8953	0.0833	0.003	875	43	724	40	1261	71	17.3	3.5

Grain #	Signal Duration	Uranium		Thorium		Th/U	equiva-lent U	$^{207}Pb/^{235}U$		$^{206}Pb/^{238}U$		Rho[1]	$^{207}Pb/^{206}Pb$		Age $^{207}Pb/^{235}U$		Age $^{206}Pb/^{238}U$		Age $^{207}Pb/^{206}Pb$		% disc.*	Uncert. wtd. disc,**
	(s)	ppm	2SE	ppm	2SE		ppm	Ratio	Prop2SE	Ratio	Prop2SE		Ratio	Prop2SE	Ma	Prop2SE	Ma	Prop2SE		Prop2SE		
172	118	82.9	3.1	6.5	0.2	0.08	84	1.052	0.048	0.1195	0.0039	0.5041	0.0656	0.0026	728	24	727	22	782	86	0.1	0
211	118	151.1	7.3	45.9	2	0.3	162	1.092	0.046	0.1205	0.0034	0.6775	0.065	0.0021	751	21	733	19	769	67	2.4	0.9
241	118	202.6	7.7	34.9	1.7	0.17	211	1.447	0.06	0.1289	0.0042	0.8678	0.0815	0.0018	907	25	781	24	1226	43	13.9	5
153	118	167	12	38.1	2.6	0.23	176	1.215	0.048	0.1338	0.0047	0.5218	0.0669	0.0024	807	22	808	27	820	74	-0.1	0
288	118	147.5	6.4	25.5	0.47	0.17	153	1.249	0.04	0.135	0.0027	0.6674	0.0675	0.0015	821	18	816	16	844	48	0.6	0.3
48	118	74.3	4.8	28.5	2.8	0.38	81	1.3	0.1	0.1358	0.0084	0.3932	0.0707	0.0057	842	46	818	48	860	170	2.9	0.5
278	118	122	23	76	12	0.62	140	1.67	0.1	0.1426	0.0089	0.9282	0.0857	0.0019	987	37	863	51	1323	43	12.6	3.4
222	118	273	27	96.6	6.6	0.35	296	1.54	0.12	0.1448	0.0095	0.9362	0.077	0.0023	925	51	868	54	1112	57	6.2	1.1
160	118	684	22	65.9	2.8	0.1	699	1.421	0.059	0.144	0.0055	0.5935	0.0731	0.0028	896	25	870	30	986	78	2.9	1
296	118	361	11	126.5	5.5	0.35	391	1.462	0.037	0.1456	0.0022	0.1012	0.0731	0.0022	913	15	876	13	1010	59	4.1	2.5
81	118	565	46	88.2	4.4	0.16	586	1.75	0.14	0.149	0.01	0.7789	0.0848	0.0047	1028	50	889	58	1310	110	13.5	2.8
275	118	690	68	56	5.3	0.08	703	1.854	0.053	0.1516	0.0039	0.525	0.0883	0.0026	1063	19	909	22	1375	56	33.9	-21.2
119	118	331	15	28.88	0.98	0.09	338	1.483	0.095	0.153	0.0071	0.5881	0.0705	0.0036	917	39	916	40	930	100	1.5	-0.4
190	118	617	2.2	60.9	1.5	0.99	76	1.449	0.066	0.1537	0.0051	0.471	0.0693	0.003	904	27	921	29	881	88	-4.5	1.4
252	118	800	68	228	15	0.29	854	2.545	0.098	0.1559	0.0077	0.9366	0.1198	0.0026	1280	28	932	43	1946	39	52.1	-23.6
163	118	299	13	629	16	2.1	447	1.54	0.064	0.1593	0.0059	0.658	0.0708	0.0024	952	25	952	33	930	68	-2.4	0.7
170	118	612	93	307	33	0.5	684	1.729	0.087	0.1621	0.0076	0.4509	0.0757	0.0034	1011	33	966	42	1051	88	8.1	-2
98	118	622	28	147.9	6.6	0.24	657	4.56	0.23	0.1623	0.0076	0.5115	0.211	0.011	1735	45	967	42	2890	80	66.5	-45.8
316	118	174.3	7.4	67.9	1.2	0.39	190	1.61	0.033	0.1623	0.0026	0.5296	0.0722	0.0013	973	13	969	15	988	37	1.9	-1.3
217	118	509	48	180	12	0.35	551	1.945	0.065	0.1636	0.0065	0.6931	0.0862	0.0026	1096	22	975	36	1339	61	27.2	-10.1
38	118	16.6	1.1	6.12	0.32	0.37	18	1.72	0.15	0.164	0.01	0.5457	0.0823	0.006	1008	57	977	58	1190	140	17.9	-3.7
25	118	254	21	27.5	1.3	0.11	260	1.7	0.2	0.166	0.011	0.5901	0.0726	0.0054	997	57	985	60	940	160	-4.8	0.8
117	118	54.6	3.1	52	2	0.95	67	1.59	0.082	0.1664	0.0085	0.5379	0.0694	0.0034	967	32	989	47	890	110	-11.1	2.1
185	118	202.2	7.7	106.7	3.2	0.53	227	1.654	0.061	0.1672	0.0052	0.5732	0.0715	0.0023	996	23	995	29	983	66	-1.2	0.4
224	118	70.7	3.2	37.2	1.2	0.53	79	1.69	0.061	0.1678	0.0042	0.4212	0.0735	0.0026	1010	22	999	23	1022	68	2.3	-1
271	118	229.3	3.3	38.18	0.91	0.17	238	1.736	0.033	0.1703	0.0029	0.5202	0.0738	0.0013	1021	12	1014	16	1032	37	1.7	-1.1
31	118	242	18	32.4	1.8	0.13	250	1.72	0.15	0.172	0.011	0.4723	0.076	0.0064	1006	57	1024	61	960	170	-6.7	1
302	118	78.5	3.9	76.1	1.8	0.97	96	1.8	0.042	0.1727	0.003	0.3958	0.0756	0.0016	1046	16	1027	16	1096	45	6.3	-4.3
209	118	751	38	230	24	0.31	805	1.966	0.078	0.1751	0.0072	0.7774	0.0819	0.0024	1106	28	1038	40	1227	58	15.4	-4.7
322	118	59.4	2.1	23.22	0.67	0.39	65	1.794	0.053	0.1747	0.0027	0.4677	0.0749	0.002	1044	20	1038	15	1059	54	2	-1.4

Grain #	Signal Duration	Uranium		Thorium		Th/U	equiva-lent U	$^{207}Pb/^{235}U$		$^{206}Pb/^{238}U$		Rho[1]	$^{207}Pb/^{206}Pb$		Age $^{207}Pb/^{235}U$		Age $^{206}Pb/^{238}U$		Age $^{207}Pb/^{206}Pb$		% disc.*	Uncert. wtd. disc,**
	(s)	ppm	2SE	ppm	2SE		ppm	Ratio	Prop2SE	Ratio	Prop2SE		Ratio	Prop2SE	Ma	Prop2SE	Ma	Prop2SE		Prop2SE		
184	118	128.8	5.9	62.9	4	0.49	144	1.802	0.076	0.1754	0.0061	0.5216	0.0749	0.0028	1044	27	1041	34	1040	74	-0.1	0
27	118	120.7	8.1	28.8	1.7	0.24	127	1.82	0.15	0.177	0.011	0.5787	0.0763	0.0053	1056	55	1046	60	1070	150	2.2	-0.4
243	118	118.8	4.7	24.55	0.97	0.21	125	1.869	0.05	0.1763	0.0043	0.3651	0.0771	0.0023	1073	18	1046	23	1115	60	6.2	-3
216	118	136.3	4.9	53.5	2	0.39	149	1.799	0.062	0.1774	0.0052	0.597	0.0734	0.0021	1042	23	1055	28	1045	56	-1	0.4
326	118	200	23	47.5	3.8	0.24	211	1.836	0.035	0.1785	0.0023	0.5125	0.0735	0.0013	1059	12	1059	13	1028	36	-3	2.4
299	118	74.1	3.2	41.9	1.1	0.57	84	2.093	0.046	0.1788	0.0033	0.4463	0.0844	0.0019	1145	15	1060	18	1307	40	18.9	-13.7
301	118	134.2	7.6	73.6	2.8	0.55	151	2.11	0.063	0.1814	0.0039	0.7014	0.0836	0.0019	1149	20	1074	21	1299	44	17.3	-10.7
179	118	117	7.8	33.1	1.9	0.28	125	1.964	0.085	0.185	0.0062	0.5567	0.0788	0.0029	1105	28	1093	34	1161	75	5.9	-2
43	118	154	9.4	50.6	2.6	0.33	166	1.95	0.18	0.187	0.012	0.679	0.0757	0.0051	1075	62	1110	65	1010	140	-9.9	15
306	118	597	50	149.6	3.4	0.25	632	2.79	0.16	0.1921	0.0098	0.954	0.1057	0.002	1349	43	1129	53	1730	33	34.7	-11.3
76	118	106.6	4.9	14.8	0.46	0.14	110	2.02	0.11	0.1934	0.0085	0.3797	0.0788	0.0044	1123	38	1137	46	1160	110	2	-0.5
84	118	22.4	1.1	21.35	0.88	0.95	27	2.75	0.23	0.194	0.011	0.7944	0.1022	0.0052	1345	60	1141	57	1657	96	31.1	-9.1
264	118	25.1	1.1	9.45	0.32	0.38	27	2.082	0.068	0.1959	0.0044	0.222	0.0784	0.0026	1142	23	1152	24	1145	68	-0.6	0.3
161	118	170.2	6	60.2	1.4	0.35	184	2.501	0.094	0.2007	0.0072	0.6033	0.0891	0.003	1279	28	1177	39	1396	64	15.7	-5.6
58	118	296	23	36	1.5	0.12	304	2.25	0.16	0.202	0.011	0.5314	0.0808	0.005	1189	49	1180	60	1180	130	0	0
110	118	24.8	1.2	9.88	0.3	0.4	27	2.17	0.12	0.2012	0.0081	0.5575	0.08	0.0035	1159	39	1180	44	1181	91	0.1	0
62	118	249	12	76.6	3.9	0.31	267	2.23	0.15	0.202	0.011	0.6506	0.0811	0.0041	1187	48	1183	57	1220	100	3	-0.6
140	118	314	28	148	12	0.47	349	2.29	0.12	0.2035	0.0093	0.6784	0.0826	0.0031	1207	38	1191	50	1254	74	5	-1.3
262	118	43.6	1.5	44.5	3.1	1.02	54	2.319	0.068	0.2055	0.004	0.5606	0.0832	0.0019	1218	20	1204	22	1278	44	5.8	-3.4
86	118	100.2	4.6	29.4	1.1	0.29	107	2.23	0.12	0.2061	0.0082	0.4861	0.0807	0.004	1177	40	1205	44	1200	100	-0.4	0.1
158	118	76.7	3.9	25.56	0.94	0.33	83	2.43	0.11	0.2068	0.0084	0.588	0.0873	0.0033	1255	33	1209	45	1351	72	10.5	-3.2
188	118	111.4	6.9	12.93	0.91	0.12	114	2.275	0.094	0.2076	0.008	0.6135	0.0793	0.0026	1202	29	1214	43	1179	64	-3	0.8
33	118	86	7	23.8	1.2	0.28	92	2.42	0.22	0.209	0.014	0.658	0.0855	0.0062	1227	64	1218	75	1260	150	3.3	-0.6
164	118	638	20	345	12	0.54	719	2.349	0.098	0.2078	0.0077	0.5754	0.0843	0.0031	1229	31	1221	41	1303	70	6.3	-2
265	118	100.1	7.2	25.5	2.3	0.25	106	2.48	0.12	0.2082	0.0076	0.9225	0.088	0.0021	1261	37	1223	40	1373	45	10.9	-3.8
290	118	12.13	0.4	3.73	0.1	0.31	13	2.49	0.12	0.2125	0.0056	0.2935	0.0857	0.0041	1274	33	1241	30	1321	85	6.1	-2.7
149	118	42.8	1.7	53.1	1.4	1.24	55	2.45	0.13	0.2129	0.0089	0.571	0.0819	0.0034	1262	36	1242	47	1230	87	-1	0.3
318	118	77.9	3.1	24.11	0.82	0.31	84	2.396	0.061	0.2123	0.0034	0.4513	0.082	0.0019	1242	18	1243	18	1243	46	0	0
194	118	132	10	71.5	6	0.54	149	2.42	0.1	0.2123	0.0087	0.6483	0.0828	0.0031	1248	30	1244	47	1239	72	-0.4	0.1
292	118	417	2.5	15.25	0.82	0.37	45	2.584	0.076	0.2157	0.0043	0.5634	0.0891	0.0021	1296	21	1258	23	1405	45	10.5	-6.4

Grain #	Signal Duration	Uranium		Thorium		Th/U	equiva-lent U	$^{207}Pb/^{235}U$		$^{206}Pb/^{238}U$		Rho[1]	$^{207}Pb/^{206}Pb$		Age $^{207}Pb/^{235}U$		Age $^{206}Pb/^{238}U$		Age $^{207}Pb/^{206}Pb$		% disc.*	Uncert. wtd. disc,**
	(s)	ppm	2SE	ppm	2SE		ppm	Ratio	Prop2SE	Ratio	Prop2SE		Ratio	Prop2SE	Ma	Prop2SE	Ma	Prop2SE		Prop2SE		
250	118	176.7	9.1	85.3	3.9	0.48	197	2.591	0.055	0.22	0.0044	0.6215	0.0846	0.0017	1301	16	1281	23	1305	39	1.8	-1
286	118	75	12	35.4	6.9	0.47	83	2.535	0.056	0.2205	0.0034	0.4172	0.0841	0.0019	1283	17	1284	18	1292	46	0.6	-0.4
207	118	248.8	8.9	82.8	2.2	0.33	268	2.971	0.091	0.2309	0.0056	0.6707	0.0938	0.0023	1396	23	1338	30	1506	46	11.2	-5.6
108	118	109.4	5.4	33.7	1.2	0.31	117	2.79	0.13	0.23	0.011	0.5312	0.0879	0.0037	1352	35	1339	54	1414	82	5.3	-1.4
146	118	140.8	7.2	43.2	1.6	0.31	151	2.75	0.14	0.2337	0.0097	0.6091	0.0873	0.0037	1347	38	1351	51	1377	80	1.9	-0.5
143	118	69.2	3.8	18.7	3.2	0.27	74	3.05	0.22	0.237	0.012	0.7413	0.0936	0.0048	1405	56	1366	61	1500	91	8.9	-2.2
68	118	137.9	7.1	48.3	1.9	0.35	149	2.83	0.17	0.238	0.013	0.5512	0.0879	0.0048	1353	47	1369	67	1370	100	0.1	0
284	118	129.7	2.1	39.6	2.2	0.31	139	2.864	0.07	0.2368	0.0046	0.7179	0.0875	0.0018	1370	18	1369	24	1370	40	0.1	0
204	118	260	13	109.4	4.3	0.42	286	2.903	0.091	0.2388	0.0065	0.6035	0.0882	0.0024	1382	24	1379	34	1381	53	0.1	-0.1
309	118	159	6.3	87.7	4.3	0.55	180	3.132	0.062	0.2387	0.0033	0.5805	0.0951	0.0018	1439	15	1379	17	1543	35	10.6	-9.6
279	118	110.2	6.9	40.1	1.7	0.36	120	2.946	0.076	0.2398	0.0047	0.6234	0.0897	0.0019	1396	20	1385	24	1417	40	2.3	-1.3
232	118	249.7	9.4	149.2	6.9	0.6	285	2.965	0.087	0.2419	0.0058	0.6557	0.0891	0.002	1395	23	1395	30	1399	43	0.3	-0.1
125	118	82.1	3.5	39.8	1.1	0.48	91	3.13	0.15	0.2481	0.0098	0.6074	0.091	0.0036	1442	37	1432	50	1457	75	1.7	-0.5
313	118	122.4	9.5	127.5	5.5	1.04	152	3.6	0.13	0.252	0.008	0.9514	0.1023	0.0018	1543	31	1447	42	1665	31	13.1	-5.2
251	118	121.2	3.3	54.5	1.1	0.45	134	3.373	0.082	0.2597	0.0048	0.5545	0.0943	0.002	1496	19	1487	25	1508	40	1.4	-0.8
70	118	132.3	8.8	52.5	2.8	0.4	145	3.41	0.2	0.264	0.012	0.5494	0.0957	0.0049	1502	48	1504	59	1514	99	0.7	-0.2
189	118	212.9	4.9	32.96	0.78	0.15	221	3.35	0.12	0.2636	0.0078	0.673	0.0922	0.0024	1487	28	1506	40	1474	50	-2.2	0.8
186	118	407	17	140.8	4.1	0.35	440	3.5	0.11	0.2654	0.008	0.6513	0.0958	0.0027	1532	26	1515	41	1543	53	1.8	-0.7
248	118	54	1.7	18.24	0.37	0.34	58	3.49	0.11	0.266	0.0053	0.5714	0.0967	0.0025	1520	24	1520	27	1551	49	2	-1.1
314	118	15.3	0.5	8.58	0.23	0.56	17	4.34	0.16	0.266	0.0051	0.4043	0.1175	0.0041	1698	31	1520	26	1907	62	20.3	-14.9
139	118	75.3	2.7	29.6	2	0.39	82	3.44	0.17	0.269	0.012	0.4842	0.0941	0.0044	1511	40	1532	61	1482	87	-3.4	0.8
103	118	65.6	2.6	49	1.6	0.75	77	3.62	0.18	0.271	0.012	0.5602	0.0997	0.0042	1556	40	1543	61	1611	79	4.2	-1.1
213	118	303	12	73	6.7	0.24	320	4.84	0.15	0.271	0.0078	0.7778	0.1299	0.003	1796	27	1549	40	2099	42	26.2	-13.8
123	118	199	14	120.6	3.9	0.61	227	3.75	0.18	0.274	0.011	0.5806	0.1011	0.0041	1587	39	1555	55	1664	76	6.6	-2
41	118	317	16	179.9	9	0.57	359	3.98	0.32	0.278	0.017	0.5616	0.1059	0.0075	1613	66	1582	86	1690	130	6.4	-1.3
238	118	148.3	9.1	34.9	1.5	0.24	157	3.642	0.1	0.2779	0.006	0.5031	0.0948	0.0025	1561	22	1584	31	1525	49	-3.9	1.9
195	118	76.7	2.7	30.1	0.87	0.39	84	3.73	0.14	0.2791	0.0088	0.5274	0.098	0.0032	1575	32	1590	43	1585	61	-0.3	0.1
34	118	126.5	8.1	36.4	1.6	0.29	135	3.68	0.27	0.285	0.016	0.5628	0.0982	0.0063	1572	60	1609	81	1530	120	-5.2	1
105	118	90.3	5.4	47	1.7	0.52	101	3.82	0.21	0.285	0.013	0.6883	0.0982	0.0042	1595	47	1620	66	1589	81	-2	0.5
268	118	230.4	3.7	128.9	6	0.56	261	4.13	0.085	0.2881	0.0044	0.6722	0.104	0.0018	1659	17	1631	22	1697	33	3.9	-3

Grain #	Signal Duration	Uranium		Thorium		Th/U	equiva-lent U	$^{207}Pb/^{235}U$		$^{206}Pb/^{238}U$		Rho[1]	$^{207}Pb/^{206}Pb$		Age $^{207}Pb/^{235}U$		Age $^{206}Pb/^{238}U$		Age $^{207}Pb/^{206}Pb$		% disc.*	Uncert. wtd. disc,**
	(s)	ppm	2SE	ppm	2SE		ppm	Ratio	Prop2SE	Ratio	Prop2SE		Ratio	Prop2SE	Ma	Prop2SE	Ma	Prop2SE		Prop2SE		
261	118	800	39	223.2	4.9	0.28	852	4.047	0.09	0.2882	0.0049	0.5914	0.1008	0.0019	1642	18	1632	24	1634	34	0.1	-0.1
277	118	120.9	5.8	311	2.2	0.26	128	4.091	0.077	0.2915	0.0049	0.531	0.1008	0.0019	1651	15	1649	24	1634	36	-0.9	0.6
18	118	262	13	92.5	3.6	0.35	284	4.24	0.31	0.293	0.016	0.5894	0.1042	0.0064	1653	60	1658	83	1680	120	1.3	-0.3
89	118	278	14	78.9	3.2	0.28	297	3.97	0.19	0.296	0.013	0.5566	0.1022	0.0045	1634	38	1665	63	1630	82	-2.1	0.6
233	118	76.4	2.7	55.6	1.4	0.73	89	4.1	0.12	0.2959	0.0072	0.5526	0.1017	0.0028	1653	24	1669	36	1649	49	-1.2	0.6
47	118	347	18	151	10	0.44	382	5.21	0.37	0.298	0.017	0.5684	0.1304	0.0082	1857	64	1672	87	2070	110	19.2	-4.6
167	118	224.5	9.6	121.8	3.3	0.54	253	4.19	0.18	0.297	0.011	0.6294	0.1044	0.0035	1671	35	1678	55	1685	62	0.4	-0.1
51	118	138.7	8	66.3	2.9	0.48	154	4.23	0.35	0.297	0.017	0.5749	0.1039	0.0069	1660	70	1679	85	1650	120	-1.8	0.3
300	118	73.5	2.9	51.5	1.6	0.7	86	4.2	0.085	0.2976	0.0044	0.6141	0.1023	0.0018	1672	17	1679	22	1665	32	-0.8	0.6
104	118	45	2.7	30	1.5	0.67	52	4.07	0.24	0.299	0.013	0.5035	0.1009	0.0051	1630	48	1682	66	1658	93	-1.4	0.4
235	118	238	23	150	11	0.63	273	4.39	0.13	0.3005	0.0075	0.6945	0.1052	0.0025	1708	24	1697	37	1709	43	0.7	-0.3
54	118	456	26	95.6	5.8	0.21	478	5.16	0.38	0.307	0.019	0.7219	0.1236	0.0069	1831	66	1729	96	1980	100	12.7	-2.6
69	118	340	17	74.4	2.7	0.22	357	4.68	0.31	0.311	0.015	0.6594	0.1107	0.0058	1747	57	1737	74	1760	99	1.3	-0.3
131	118	117.9	8	39.73	0.97	0.34	127	4.88	0.25	0.312	0.014	0.7976	0.115	0.004	1797	44	1743	72	1869	61	6.7	-1.8
307	118	126.6	4.8	35.14	0.86	0.28	135	4.546	0.099	0.3114	0.0056	0.5558	0.1055	0.0019	1740	18	1747	28	1723	34	-1.4	0.9
29	118	208	12	51.1	3.9	0.25	220	4.38	0.37	0.314	0.02	0.5522	0.1033	0.0078	1671	70	1760	100	1630	140	-8	1.3
297	118	63.8	2.4	76.8	2.2	1.2	82	4.814	0.1	0.3173	0.0048	0.4281	0.1092	0.0022	1785	18	1776	24	1790	39	0.8	-0.6
93	118	247	41	32	2.2	0.13	255	4.6	0.27	0.318	0.015	0.5307	0.1066	0.0057	1737	48	1780	74	1710	100	-4.1	0.9
249	118	175.2	4	52.5	1	0.3	188	4.99	0.13	0.3289	0.0072	0.6176	0.11	0.0023	1817	23	1836	34	1798	38	-2.1	1.1
287	118	157.7	5.6	69.4	1.9	0.44	174	5.266	0.11	0.3317	0.0052	0.5919	0.1158	0.0021	1866	17	1846	25	1889	32	2.3	-1.7
182	118	203.8	7.7	52.7	1.7	0.26	216	5.22	0.21	0.334	0.012	0.6462	0.1146	0.0039	1848	34	1855	57	1862	62	0.4	-0.1
50	118	96.9	5.4	37.5	1.8	0.39	106	5.5	0.41	0.338	0.021	0.622	0.1197	0.008	1886	66	1864	99	1920	120	2.9	-0.6
133	118	156	16	57.3	4.1	0.37	169	5.19	0.23	0.337	0.012	0.5551	0.1145	0.0047	1849	38	1866	57	1852	75	-0.8	0.2
267	118	72.1	4.3	0.64	0.03	0.01	72	5.23	0.12	0.3374	0.0067	0.5653	0.1117	0.0024	1855	20	1873	32	1820	38	-2.9	1.7
90	118	232.4	8.6	66.5	2.7	0.29	248	5.48	0.31	0.34	0.014	0.6199	0.1173	0.0052	1885	49	1879	69	1905	80	1.4	-0.4
111	118	139.8	9.6	26.62	0.82	0.19	146	5.29	0.25	0.342	0.015	0.6324	0.1143	0.0043	1862	39	1890	71	1871	70	-1	0.3
181	118	273.8	8.9	136.9	4.1	0.5	306	5.67	0.22	0.341	0.013	0.5903	0.1205	0.004	1923	35	1895	61	1963	61	3.5	-1.1
49	118	46.1	2.6	36.6	1.7	0.79	55	5.88	0.51	0.344	0.022	0.6307	0.1179	0.0082	1912	76	1910	110	1890	130	-1.1	0.2
230	118	299	13	224.2	6.6	0.75	352	5.66	0.15	0.35	0.0075	0.6745	0.1172	0.0024	1925	24	1933	36	1914	38	-1	0.5
191	118	302	17	1.59	0.06	0.01	302	6.4	0.22	0.362	0.011	0.6451	0.1266	0.0037	2034	30	2002	51	2046	51	2.2	-0.9

Grain #	Signal Duration	Uranium		Thorium		Th/U	equiva-lent U	$^{207}Pb/^{235}U$		$^{206}Pb/^{238}U$		Rho[1]	$^{207}Pb/^{206}Pb$		Age $^{207}Pb/^{235}U$		Age $^{206}Pb/^{238}U$		Age $^{207}Pb/^{206}Pb$		% disc.*	Uncert. wtd. disc,**
	(s)	ppm	2SE	ppm	2SE		ppm	Ratio	Prop2SE	Ratio	Prop2SE		Ratio	Prop2SE	Ma	Prop2SE	Ma	Prop2SE		Prop2SE		
75	118	220	11	57.6	2.1	0.26	234	6.27	0.42	0.364	0.019	0.5467	0.1258	0.007	1994	59	2003	93	2035	100	1.6	-0.3
319	118	115.1	5.1	31.3	2.3	0.27	122	6.61	0.14	0.3756	0.0061	0.5783	0.126	0.0023	2058	19	2055	28	2042	33	-0.6	0.5
118	118	263	16	74.9	2.3	0.28	281	7.56	0.43	0.401	0.019	0.681	0.1386	0.006	2160	52	2175	86	2210	77	1.6	-0.4
225	118	43.5	1.3	22.1	0.5	0.51	49	9.07	0.28	0.412	0.012	0.7502	0.1613	0.0036	2343	28	2218	55	2468	39	10.1	-4.5
255	118	607	30	161.3	9.1	0.27	645	9.7	0.24	0.4293	0.0088	0.7919	0.1635	0.003	2404	23	2300	40	2491	30	7.7	-4.8
83	118	68	3.1	58.4	2.4	0.86	82	12.01	0.78	0.47	0.024	0.6314	0.1876	0.0097	2601	60	2480	110	2703	89	8.3	-2
236	118	93.8	4.5	92.8	2.5	0.99	116	11.35	0.31	0.473	0.012	0.709	0.1726	0.0036	2552	25	2493	50	2583	34	3.5	-1.8
42	118	590	41	229	15	0.39	644	20.6	1.9	0.501	0.037	0.6665	0.306	0.023	3125	91	2590	160	3440	120	24.7	-5.3
165	118	37.5	1.2	28.5	1.3	0.76	44	14.67	0.58	0.549	0.018	0.5332	0.1956	0.0069	2788	38	2813	77	2796	56	-0.6	0.2
187	118	46.7	3.5	44.7	3.9	0.96	57	14.05	0.61	0.55	0.02	0.6767	0.1857	0.0063	2751	43	2819	82	2689	55	-4.8	1.6
141	118	105.3	8.9	14.8	0.5	0.14	109	15.63	0.73	0.571	0.024	0.6818	0.2019	0.0075	2857	44	2902	98	2823	60	-2.8	0.8
35	118	344	29	117	11	0.34	371	20.7	1.7	0.576	0.037	0.5989	0.275	0.02	3112	80	2920	150	3250	120	10.2	-2.2
71	118	124	6.2	40.6	1.5	0.33	134	35.8	2.1	0.769	0.039	0.5264	0.346	0.019	3664	61	3650	140	3671	87	0.6	-0.2

Footnotes: Rows in grey indicate discordant data not used for calculations or plots.
1: Rho, $^{206}Pb/^{238}U$ vs. $^{207}Pb/^{235}U$ error correlation
*** % Disc.: Discordance in % is calculated as = (1- ($^{206}Pb/^{238}U$ date / $^{207}Pb/^{235}U$ date)) x 100 for dates younger than 1000 Ma, and as = (1- ($^{206}Pb/^{238}U$ date / $^{207}Pb/^{206}Pb$ date)) x 100 for dates older than 1000 Ma.**
A value of 1.2 for the uncertainty weighted age difference was used as discordance cut-off for dates younger than 1000 Ma. For dates older than 1000 Ma, data more discordance than 5% were excluded.
**** Uncert. wtd. disc,: The uncertainty weighted age difference is calculated as: ($^{207}Pb/^{235}U$ date - $^{206}Pb/^{238}U$ date) / Prop 2SE $^{207}Pb/^{235}U$ date**

Appendix B: $\delta^{13}C_{org}$ Analyses

$\delta^{13}C$ Analyses of the Wayan Formation

Analysis #	Sample #	Amount (mg)	Ampl 44 (mV)	Area 44 (Vs)	$\delta^{13}C$ VPDB	C%
110557	0.0	15.733	1164	26.60	-23.32	0.10
110558	0.5	28.725	2550	58.04	-24.95	0.12
110559	1.0	19.485	1475	33.03	-23.41	0.10
110870	1.5	30.665	2904	66.89	-25.71	0.11
110561	2.0	19.258	8993	202.27	-8.15	0.60
110562	2.5	16.602	1629	37.24	-23.69	0.13
110563	3.0	3.016	1146	26.58	-23.14	0.50
110564	3.5	16.843	797	18.27	-24.23	0.06
110871	4	30.373	1221	28.15	-24.85	0.04
110872	4.5	31.794	1697	38.82	-24.68	0.06
110569	5.0	17.099	1365	31.04	-24.64	0.10
110570	5.5	3.173	809	18.43	-15.23	0.33
110572	6.0	4.396	3048	68.16	-9.75	0.88
110873	6.5	28.739	2987	68.96	-24.00	0.13
110874	7	31.048	1528	35.07	-24.03	0.06
110875	7.5	30.389	1543	35.14	-24.10	0.06
110578	8.0	4.373	688	15.88	-24.37	0.21
110579	8.5	30.122	22158	517.31	-3.73	0.98
110580	9.0	17.848	1152	26.80	-26.49	0.09
110876	9.5	19.452	2484	57.06	-25.72	0.15
110582	10.0	4.166	1884	42.27	-8.49	0.58
110583	10.5	15.937	679	15.44	-24.51	0.06
110877	11	33.238	1517	34.90	-25.94	0.05
111179	11.5	31.100	1652	36.76	-25.45	0.06
110588	12.0	25.765	1616	36.89	-24.42	0.08
110589	12.5	25.733	2428	55.17	-24.50	0.12
110590	13.0	25.240	1343	30.57	-23.77	0.07
110591	13.5	28.203	3280	74.19	-24.64	0.15
110592	14.0	29.192	6533	146.55	-17.47	0.29
110881	14.5	30.584	7594	175.61	-24.54	0.31
110882	15.0	30.044	8352	190.53	-23.13	0.34
110883	15.5	30.422	8300	188.98	-22.00	0.34
110885	16.0	30.720	10628	242.96	-16.31	0.43
110886	16.5	36.781	33825	804.94	-5.85	1.20
110887	17.0	31.924	29382	699.20	-7.62	1.20
110888	17.5	30.656	25680	607.84	-2.98	1.09
110891	18.0	30.236	10557	241.70	-8.24	0.43
110892	18.5	30.746	3122	71.28	-25.42	0.12
110893	19.0	30.596	3179	72.45	-25.24	0.12
110894	19.5	30.728	2158	49.67	-25.48	0.08
110895	20.0	30.373	7145	164.68	-25.51	0.29
110896	20.5	30.584	5373	122.67	-25.72	0.21
110897	21.0	30.594	1991	45.61	-26.75	0.07
110898	21.5	30.174	6400	146.11	-17.79	0.26
110901	22.0	30.578	2737	62.12	-26.79	0.10
110902	22.5	30.056	43026	1104.68	-9.37	2.02
110903	23.0	30.318	2585	58.18	-26.03	0.10
110904	23.5	32.266	906	20.72	-26.69	0.03
110905	24.0	34.594	1681	37.87	-25.59	0.05
111180	24.5	30.850	1425	31.70	-25.97	0.05
111181	25.0	30.359	3965	88.33	-26.57	0.16
111182	25.5	30.452	4559	102.84	-17.20	0.18
111183	26.0	30.565	1751	39.22	-25.80	0.07
111184	26.5	33.812	1944	43.70	-27.07	0.07
111185	27.0	36.400	2751	62.40	-26.91	0.09

Footnote: Rows in grey indicate samples that were not fully decarbed, or did not fully combust.
Sample # indicates the sample location in meters from the base of the measured section.

Appendix C: $\delta^{13}C$ and $\delta^{18}O$ Analyses

$\delta^{13}C$ and $\delta^{18}O$ Analyses of Wayan Formation Carbonate Nodules

Sample[1]	$\delta^{13}C$ (KIS)	±	$\delta^{18}O$ (KIS)	±	$\delta^{13}C$ (VPDB)	$\delta^{18}O$ (VPDB)	Max P
WN-1.2 NLSVC	-4.35	0.06	-4.44	0.11	-7.95	-8.72	958
WN-1.2 NLSVC	-4.37	0.01	-4.32	0.02	-7.96	-8.60	1178
WN-1.2 NLSVC	-4.71	0.02	-3.71	0.05	-8.30	-7.99	1060
WN-1.2 NLSVC	-3.84	0.02	-5.52	0.06	-7.44	-9.80	1058
WN-1.2 NLSVC	-4.45	0.02	-4.12	0.03	-8.05	-8.39	1060
WN-1.2 DLSVC	-4.29	0.01	-4.32	0.03	-7.89	-8.60	1200
WN-1.2 DLSVC	-4.50	0.01	-3.83	0.01	-8.10	-8.11	1163
WN-1.2 DLSVC	-5.01	0.01	-3.67	0.02	-8.60	-7.94	1183
WN-1.2 DLSVC	-4.19	0.01	-4.88	0.01	-7.78	-9.16	1202
WN-1.2 DLSVC	-5.15	0.01	-3.68	0.01	-8.74	-7.96	1161
WN-1.2 BLSVC	-2.57	0.03	-11.31	0.04	-6.18	-15.61	1073
WN-1.2 BLSVC	-2.61	0.06	-11.84	0.13	-6.23	-16.14	1236
WN-1.2 BLSVC	-3.09	0.01	-12.26	0.02	-6.70	-16.56	1205
WN-1.2 BLSVC	-2.87	0.02	-12.20	0.02	-6.48	-16.50	1192
WN-1.2 BLSVC	-3.09	0.06	-11.81	0.10	-6.70	-16.10	1246
WN-1.2 SRFMM	-4.00	0.01	-4.34	0.03	-7.60	-8.61	1161
WN-1.2 SRFMM	-4.83	0.01	-4.55	0.02	-8.42	-8.83	1134
WN-1.2 SRFMM	-4.77	0.01	-4.82	0.02	-8.36	-9.09	1090
WN-1.2 SRFMM	-4.79	0.02	-4.85	0.03	-8.38	-9.13	1200
WN-1.2 SRFMM	-4.73	0.06	-4.82	0.15	-8.32	-9.10	1212
WN-1.3 DLSVC	-4.05	0.01	-4.27	0.03	-7.65	-8.55	1165
WN-1.3 DLSVC	-4.27	0.06	-4.24	0.08	-7.87	-8.52	1248
WN-1.3 DLSVC	-3.96	0.00	-4.33	0.02	-7.56	-8.60	1207
WN-1.3 DLSVC	-3.89	0.01	-4.05	0.03	-7.49	-8.32	1090
WN-1.3 DLSVC	-4.38	0.01	-3.73	0.01	-7.98	-8.01	1197
WN-1.3 BLSVC	-5.33	0.03	-9.72	0.05	-8.92	-14.01	1266
WN-1.3 BLSVC	-4.06	0.01	-9.23	0.01	-7.66	-13.52	1209
WN-1.3 BLSVC	-4.79	0.01	-9.51	0.01	-8.39	-13.81	1207
WN-1.3 BLSVC	-4.93	0.03	-9.46	0.09	-8.52	-13.75	1214
WN-1.3 BLSVC	-4.13	0.01	-6.71	0.04	-7.72	-10.99	1146
WN-1.3 DLMM	-3.74	0.09	-4.16	0.12	-7.34	-8.43	1241
WN-1.3 DLMM	-3.53	0.01	-4.63	0.01	-7.13	-8.91	1180
WN-1.3 DLMM	-3.74	0.06	-4.31	0.11	-7.35	-8.59	1236
WN-1.3 DLMM	-3.83	0.01	-4.14	0.01	-7.43	-8.42	1185
WN-1.3 DLMM	-3.93	0.01	-4.08	0.02	-7.53	-8.36	1158
WN-1.3 NLMN	-4.04	0.04	-3.95	0.06	-7.64	-8.23	1248
WN-1.3 NLMN	-4.39	0.01	-3.95	0.02	-7.99	-8.23	1205
WN-1.3 NLMN	-3.98	0.06	-4.07	0.07	-7.58	-8.35	1244
WN-1.3 NLMN	-4.19	0.01	-3.91	0.02	-7.79	-8.19	1056
WN-1.3 NLMN	-4.02	0.07	-4.09	0.13	-7.62	-8.36	1244
WN-1.5 BLSVC	-4.06	0.01	-5.09	0.02	-7.66	-9.37	1202
WN-1.5 BLSVC	-2.87	0.01	-11.52	0.02	-6.48	-15.82	1070
WN-1.5 BLSVC	-2.66	0.05	-11.78	0.15	-6.27	-16.08	1219
WN-1.5 BLSVC	-2.73	0.06	-11.51	0.12	-6.34	-15.81	1219
WN-1.5 BLSVC	-3.02	0.02	-11.04	0.05	-6.63	-15.34	1100
WN-1.5 LSVC	-3.87	0.06	-4.74	0.06	-7.47	-9.01	1229
WN-1.5 LSVC	-3.84	0.04	-4.29	0.11	-7.44	-8.56	1253
WN-1.5 LSVC	-3.59	0.05	-4.96	0.10	-7.19	-9.24	1261
WN-1.5 LSVC	-4.33	0.01	-4.24	0.02	-7.93	-8.52	1187
WN-1.5 LSVC	-3.80	0.01	-6.52	0.02	-7.40	-10.80	1158
WN-1.5 SRFMM	-4.35	0.01	-3.93	0.01	-7.95	-8.21	1185
WN-1.5 SRFMM	-4.39	0.01	-4.11	0.02	-7.99	-8.39	1214
WN-1.5 SRFMM	-5.05	0.01	-3.61	0.02	-8.64	-7.88	1173
WN-1.5 SRFMM	-4.21	0.03	-3.66	0.04	-7.80	-7.94	1102
WN-1.5 SRFMM	-4.26	0.01	-3.67	0.02	-7.86	-7.95	1104
WN-1.5 NLSVC	-4.63	0.03	-3.25	0.07	-8.22	-7.53	1263
WN-1.5 NLSVC	-5.05	0.01	-3.81	0.02	-8.64	-8.09	1131

Footnote: 1. NLSVC: non-luminescent septarian vein calcite; DLSVC: dully luminescent septarian vein calcite; BLSVC: brightly luminescent septarian vein calcite; SRFMM: speckled radial fibrous microspar matrix; DLMM: dully luminescent micritic matrix; NLMN: non-luminescent micritic nodule; LSVC: luminescent septarian vein calcite.